

การตรวจสอบการคำนวณปริมาณรังสีของวิธีมอนติคาร์โลในเครื่องวางแผนการรักษาของลำอิเล็ก
ตรอนขนาดเล็ก



นายมิน ปิว หวง

จุฬาลงกรณ์มหาวิทยาลัย

CHULALONGKORN UNIVERSITY

วิทยานิพนธ์นี้เป็นส่วนหนึ่งของการศึกษาตามหลักสูตรปริญญาวิทยาศาสตรมหาบัณฑิต

สาขาวิชาอายุเวชศาสตร์ ภาควิชารังสีวิทยา

คณะแพทยศาสตร์ จุฬาลงกรณ์มหาวิทยาลัย

ปีการศึกษา 2556


ลิขสิทธิ์ของจุฬาลงกรณ์มหาวิทยาลัย

บทคัดย่อและแฟ้มข้อมูลฉบับเต็มของวิทยานิพนธ์ตั้งแต่ปีการศึกษา 2554 ที่ให้บริการในคลังปัญญาจุฬาฯ (CUIR)

เป็นแฟ้มข้อมูลของนิสิตเจ้าของวิทยานิพนธ์ ที่ส่งผ่านทางบัณฑิตวิทยาลัย

The abstract and full text of theses from the academic year 2011 in Chulalongkorn University Intellectual Repository (CUIR) are the thesis authors' files submitted through the University Graduate School.

DOSE VERIFICATION OF SMALL FIELD ELECTRON BEAM CALCULATED BY MONTE
CARLO ALGORITHM IN COMMERCIAL TREATMENT PLANNING

The emblem of Chulalongkorn University, featuring a central figure holding a sword, surrounded by a sunburst of rays, all resting on a decorative base.

Mr. Minh Bui Hoang

จุฬาลงกรณ์มหาวิทยาลัย

CHULALONGKORN UNIVERSITY

A Thesis Submitted in Partial Fulfillment of the Requirements
for the Degree of Master of Science Program in Medical Imaging

Department of Radiology

Faculty of Medicine

Chulalongkorn University

Academic Year 2013

Copyright of Chulalongkorn University

Thesis Title	DOSE VERIFICATION OF SMALL FIELD ELECTRON BEAM CALCULATED BY MONTE CARLO ALGORITHM IN COMMERCIAL TREATMENT PLANNING
By	Mr. Minh Bui Hoang
Field of Study	Medical Imaging
Thesis Advisor	Associate Professor Sivalee Suriyapee, M.eng.
Thesis Co-Advisor	Taweap Sanghangthum, Ph.D.

Accepted by the Faculty of Medicine, Chulalongkorn University in Partial Fulfillment
of the Requirements for the Master's Degree

..... Dean of the Faculty of Medicine
(Associate Professor Sophon Napathorn, M.D.)

THESIS COMMITTEE

..... Chairman
(Associate Professor Kanjana Shotelersak, M.D.)

..... Thesis Advisor
(Associate Professor Sivalee Suriyapee, M.eng.)

..... Thesis Co-Advisor
(Taweap Sanghangthum, Ph.D.)

..... External Examiner
(Professor Franco Milano)

CHULALONGKORN UNIVERSITY

มี น บิ ว ห ว ง :
 การตรวจสอบการคำนวณปริมาณรังสีของวิธีมอนติคาร์โลในเครื่องวางแผนการรักษาของ
 ลำอิเล็กตรอนขนาดเล็ก. (DOSE VERIFICATION OF SMALL FIELD ELECTRON
 BEAM CALCULATED BY MONTE CARLO ALGORITHM IN COMMERCIAL
 TREATMENT PLANNING) อ.ที่ปรึกษาวิทยานิพนธ์หลัก: รศ. ศิวลี สุริยาปี, วศม.,
 อ.ที่ปรึกษาวิทยานิพนธ์ร่วม: ดร. ทวีป แสงแห่งธรรม, วศด., 4 หน้า.

วัตถุประสงค์ของงานวิจัยนี้เพื่อตรวจสอบความถูกต้องในการคำนวณปริมาณรังสีของลำ
 อิเล็กตรอนขนาดเล็กของเครื่องวางแผนการรักษา Eclipse
 ที่ใช้การคำนวณแบบอิเล็กตรอนมอนติคาร์โล (eMc)
 โดยทำการเปรียบเทียบค่าปริมาณรังสีตามความลึกปริมาณรังสีตามแนวระนาบ สัดส่วนเอทพุท
 และการกระจายรังสี ระหว่างค่าที่คำนวณได้จาก Eclipse และค่าที่วัดได้จริงด้วยไดโอดและฟิล์ม
 EDR2 ทำการศึกษาที่อิเล็กตรอนพลังงาน 6 12 และ 20 ล้านอิเล็กตรอนโวลต์
 และขนาดคัทเอทเล็กๆ จากการทดลองพบว่าค่าความแตกต่างของปริมาณรังสีตามความลึก
 ปริมาณรังสีตามแนวระนาบ สัดส่วนเอทพุทระหว่างค่าที่คำนวณกับค่าที่วัดได้อยู่ภายในขีดจำกัด
 2% และ 2 มม. และมีค่าการผ่านแกมมาสำหรับการกระจายรังสีมากกว่า 93%
 ในทุกพลังงานและทุกขนาดคัทเอทสี่เหลี่ยมตั้งแต่ 3x3 ถึง 10x10 ซม.²
 อย่างไรก็ตามที่คัทเอทขนาด 1x1 และ 2x2 ซม.² พบค่าความแตกต่างมากกว่าขีดจำกัด
 และมีค่าการผ่านแกมมาต่ำกว่า 90%
 ในส่วนคัทเอทรูปร่างผิดปกติแบบต่างๆ และมีด้านหนึ่งที่มีขนาดเล็ก
 พบว่าค่าปริมาณรังสีตามความลึกปริมาณรังสีตามแนวระนาบและสัดส่วนเอทพุทไม่แตกต่างจาก
 ค่าที่ได้จากคัทเอทมาตรฐานสี่เหลี่ยมที่มีด้านเท่ากับด้านขนาดเล็กของคัทเอทรูปร่างผิดปกติอย่าง
 งามนี้ ย ส ำ ค ัญ (น ้อ ย ก ว ำ 2 %)
 จากการทดลองชี้ให้เห็นว่าการคำนวณอิเล็กตรอนโดยวิธีมอนติคาร์โลสามารถนำมาหาค่าปริมาณรัง
 สี ต ำ ม ค ว ำ ม ลี ก ป ริ ม ำ ณ ร ัง สี ต ำ ม แ น ว ร ะ น ำ บ
 ส ั ด ส ่ว น เ อ ท พุ ท ได ้อ ย ำ ง ถู ก ต ้อง ส ำ ห รั บ ข น ำ ด ค ัท เ อ ท ที่ น ้อ ย ที่ ส ู ด ถึ ง 3 ซม.
 ส ำ ห รั บ ล ำ อิ ล ั ก ต ร ็ อ น พ ล ั ง ง ำ น 6 , 1 2 แ ล ะ 2 0 ล ำ น อิ ล ั ก ต ร ็ อ น โ ว ล ์
 ก ำ ร ค ำ น ว ำ น อิ ล ั ก ต ร ็ อ น ม ็ อ น ตี ค ำ ร โ ล ใน โ ป ร แ ก ร ม ว ำ ง แ พ ะ น ก ำ ร ร ั ก ข ำ E c l i p s e
 มี ความ ถูก ต ้อง ใน ก ำ ร ค ำ น ว ำ น ม ำ ก ก ำ ร ค ำ น ว ำ น เ ว อร์ ช ัน ก ่อน ห ำ
 โดยเฉพาะลำรังสีขนาดเล็กในตัวอย่างที่สม่ำเสมอ

ภาควิชา รังสีวิทยา

สาขาวิชา ฉายาเวชศาสตร์

ปีการศึกษา 2556

ลายมือชื่อนิสิต

ลายมือชื่อ อ.ที่ปรึกษาวิทยานิพนธ์หลัก

ลายมือชื่อ อ.ที่ปรึกษาวิทยานิพนธ์ร่วม

5574211130 : MAJOR MEDICAL IMAGING

KEYWORDS: ELECTRON BEAMS / SMALL FIELDS / MONTE CARLO / DOSE
VERIFICATION / TREATMENT PLANNING

MINH BUI HOANG: DOSE VERIFICATION OF SMALL FIELD ELECTRON BEAM
CALCULATED BY MONTE CARLO ALGORITHM IN COMMERCIAL TREATMENT
PLANNING. ADVISOR: ASSOC. PROF. SIVALEE SURIYAPEE, M.ENG.,TAWEAP
SANGHANGTHUM, Ph.D., 4 pp.

The purpose of this study is to verify dosimetric accuracy of Electron Monte Carlo (eMC) algorithm in Eclipse treatment planning for small field electron beams by comparing eMC calculations and measurements of percentage depth doses, beam profile, output factor and isodose distributions for 6, 12 and 20 MeV with small cutout size combinations. Measurements were made using EDR2 film and diode detector–EFD10025. All comparisons of percentage depth doses, beam profile, output factor, isodose distribution matched well within tolerance of 2% and 2 mm, gamma pass were greater than 93% for all of tested energies in the case of square field sizes cutout from 3x3 to 10x10 cm². However, The 1x1 and 2x2 cm² cutout presented the worst results of running-out the tolerance, gamma pass were below 90%. The comparison of percentage depth dose, output factors and dose distribution for irregular shape of one dimension of the shape field which was equal to small square fields were not significantly different with standard shape (less than 2%). Our results indicated that the eMC algorithm can accurately predict percentage depth doses, beam profiles and output factor for field sizes as small as 3.0 cm diameter for energies in the 6, 12 and 20 MeV. The Monte Carlo algorithm for electron planning in Eclipse is more accurate than previous algorithms for small field sizes in homogenous media

Department: Radiology

Student's Signature

Field of Study: Medical Imaging

Advisor's Signature

Academic Year: 2013

Co-Advisor's Signature

ACKNOWLEDGEMENTS

I would like to express gratitude and deepest appreciation to Assoc. Prof. Sivalee Suriyapee, Chief Physicist at Division of Therapeutic Radiology and Oncology, Department of Radiology, Faculty of Medicine, Chulalongkorn University, my major advisor for her guidance, invaluable advice, supervision, constructive comments, and English language proof in this research. I am equally grateful to Dr.Taweap Sanghangthum my co-advisor for his help in the experiment, kind suggestion, and constructive comments in the experiments and English language proof in this research.

I would like to express sincere thanks to Assoc.Prof.Anchali Krisanachinda, Chair, Medical Imaging Graduate Program, Chulalongkorn University for constructive advice and comments in the research proposal.

I am grateful to all teachers and lecturers, in School of Medical Imaging and staff at Division of Therapeutic Radiology and Oncology, King Chulalongkorn Memorial Hospital for their kind support and supply the knowledge in Medical Imaging. I also wish to thank my friends in School of Chulalongkorn University for their help and encouragement thought the entire course of study.

Finally, I have to sincerely regard mention to my mother, my father for their infinite love, assistance, carefulness and entirely support throughout my whole study. The productiveness of this thesis, I dedicate to my family and all teachers who taught me since my childhood.

CONTENTS

	Page
THAI ABSTRACT.....	iv
ENGLISH ABSTRACT	v
ACKNOWLEDGEMENTS	vi
CONTENTS.....	vii
LIST OF TABLES.....	x
LIST OF FIGURE.....	xii
LIST OF ABBREVIATIONS.....	xvi
CHAPTER 1 INTRODUCTION	1
1.1. Background and Rationale.....	1
1.2. Research Objectives.....	4
CHAPTER 2 LITERATURE REVIEWS	5
2.1. Theories	5
2.1.1. Energy Parameters of the Electron beam.....	5
2.1.2. Physical Characteristics of Electron Beam	8
2.1.2.1. Percentage Depth Dose (PDD).....	8
2.1.2.2. Beam Profile	10
2.1.2.3. Output Factor (OF).....	12
2.1.2.4. Isodose Distributions	13
2.1.2.5. Shaping the Beam	15
2.1.2.6. Field Size Dependence	15
2.1.3. Gamma Index Method.....	19
2.1.4. Electron Dosimeter	21
2.1.4.1. Silicon Diodes	21
2.1.4.2. Film	22
2.1.5. Electron Monte Carlo Algorithm.....	23
2.1.5.1. Initial Phase Space model (IPS).....	24
2.1.5.2 Transport model (MMC).....	25

	Page
2.1.5.3. Beam Data Measurements for The eMC Algorithm	28
2.1.5.4. eMC Calculation Options	29
CHAPTER 3 RESEARCH METHODOLOGY	33
3.1. Research design	33
3.2. Research design model	33
3.3. Conceptual framework	34
3.4. Key word.....	34
3.5. Research Questions	35
3.6 Materials.....	35
3.6.1. Eclipse treatment planning system	35
3.6.2. Linear Accelerator	36
3.6.3. Cutout Shields	38
3.6.4. Diode detector	39
3.6.5. Electrometer	40
3.6.6. WP1D water phantom	41
3.6.7. Blue water phantom	42
3.6.8. Kodak Extended Dose Range 2 (EDR2) film	43
3.6.9. Solid water phantom	44
3.6.10. Vidar model VXR-16 scanner	45
3.7 Method.....	46
3.7.1 Calculations	47
3.7.2. Measurements and Verifications for Square Fields	48
3.7.2.1. Percentage depth dose	48
3.7.2.2. Beam profile	48
3.7.2.3. Output factors	49
3.7.2.4. Dose distribution	50
3.7.3. Measurements and Verifications for Small Irregular Fields	52

	Page
CHAPTER 4 RESULTS AND DISCUSSION	53
4.1. Square Fields	53
4.1.1. Percentage Depth Dose	53
4.1.2. Beam Profiles	55
4.1.3. Output factors	61
4.1.4. Dose distributions	66
4.2. Irregular fields	70
CHAPTER 5 CONCLUSIONS	79
REFERENCES	82
VITA	86

LIST OF TABLES

	Page
Table 3. 1. The collimator jaws opening (cm^2) for given cone sizes.	37
Table 3. 2. Eclipse electron Monte Carlo calculation parameters setup.	47
Table 3. 3. Irregular field shape of cutouts.	52
Table 4. 1. Mean distance discrepancies in PDD (in mm) between calculated and measured dose evaluated at 5% intervals between 20% and 80% dose range for beams of energies 6, 12, and 20 MeV.	54
Table 4.2- a. Comparisons of calculated and measured beam profiles for 6 MeV in term of RW_{50} , \bar{d}_2 , \bar{d}_3 , \bar{d}_{50-90} for cutouts of 1x1, 2x2, 3x3, 4x4, 5x5 and 10x10 cm^2	59
Table 4.2- b. Comparisons of calculated and measured beam profiles for 12 MeV in term of RW_{50} , \bar{d}_2 , \bar{d}_3 , \bar{d}_{50-90} for cutouts of 1x1, 2x2, 3x3, 4x4, 5x5 and 10x10 cm^2	59
Table 4.2- c. Comparisons of calculated and measured beam profiles for 20 MeV in term of RW_{50} , \bar{d}_2 , \bar{d}_3 , \bar{d}_{50-90} for cutouts of 1x1, 2x2, 3x3, 4x4, 5x5 and 10x10 cm^2	60_Toc382317522
Table 4. 3. Measurement of output factors for 6, 12 and 20 MeV for square fields of cutout from 1x1 to 9x9 cm^2	61
Table 4. 4. Percentage output factors differences between calculated and measured for cutout sizes from 2x2 to 9x9 cm^2	66
Table 4. 5. Gamma pass results of dose distribution for beams energy of 6, 12 and 20 MeV with cutout sizes of 10x10, 4x4, 3x3, 2x2 and 1x1 cm^2	69
Table 4. 6. Measurements and eMC calculations of output factors for 6, 12 and 20 MeV for irregular shapes of cutout.	71
Table 4. 7. Comparison for output factors, percentage depth dose and dose distribution between measurements and eMC calculations for irregular shapes of cutout for 6, 12 and 20 MeV.	72

- Table 4. 8.** Comparison for output factors, percentage depth dose, dose distribution between measurements and eMC calculations for 1x1, 2x2, 3x3 and 4x4 cm²76
- Table 4. 9.** Comparison between square and irregular shapes in term of agreement between measurements and eMC calculations for output factors, percentage depth dose and dose distribution77



LIST OF FIGURE

	Page
Figure 1. 1. Field size of 1x1, 2x2, 3x3, 4x4, 10x10 cm ² cutout	1
Figure 1. 2. (a) Output factor and (b) Percent depth dose in small field electron beams.	2
Figure 1. 3. Beam profile of field 1x1 cm ² electron beams for 6 MeV.	3
Figure 2. 1. Electron beam energy parameters considered in the accelerator phantom geometry [2].	6
Figure 2. 2. Percentage depth dose curve of electron beam in a water phantom. .	9
Figure 2. 3. Central axis percent depth dose distribution measured in water for the 4-MeV, 6-MeV, 9-MeV, and 12-MeV electron beams.	10
Figure 2. 4. Depth dose profile showed variation of dose across the field. Dotted line indicates geometric field boundary at a 10 cm depth.	11
Figure 2. 5. The parameters used to compare beam profiles.	12
Figure 2. 6. Film used for obtaining isodose curves, exposed to 12 MeV electron beam.	13
Figure 2. 7. Cross-sectional isodose curves in a plane perpendicular to central axis [9].	14
Figure 2. 8. Variation of relative dose at d _m , through a 10 x 10 cm ² cone, with the change of jaw setting, relative to the recommended jaw setting [12].	16
Figure 2. 9. Output factors as a function of side of square field. Primary collimator fixed secondary collimators (trimmers) close to the phantom varied to change the field size [13].	17
Figure 2. 10. Variation of depth dose distribution with field size of a) 8 MeV and b) 32 MeV [14].	18
Figure 2. 11. Geometric representation of dose distribution evaluation criteria using the gamma passes technique.	19
Figure 2. 12. Schematic representation of the four sub-sources used by the IPS model [3]: 1) main photons and electrons, 2) edge electrons, 3) transmission photons and 4) secondary photons and electrons.	24

Figure 2. 13.	Local geometry used in MMC.....	25
Figure 2. 14.	Primary electron transport.....	26
Figure 2. 15.	Secondary particle transport.....	27
Figure 3. 1.	Research design model.....	33
Figure 3. 2.	Conceptual framework.....	34
Figure 3. 3.	Eclipse treatment planning software (version 8.9.21).....	36
Figure 3. 4.	Varian Clinac iX linear accelerator (Varian Medical Systems, Palo Alto, CA).....	37
Figure 3. 5.	The various shape and size of cutout shields insert in a $10 \times 10 \text{ cm}^2$ standard cone.....	38
Figure 3. 6.	The $10 \times 10 \text{ cm}^2$ standard cone of Clinac iX linear accelerator.....	39
Figure 3. 7.	The Diode Detector– EFD10025 (IBA Dosimetry GmbH, Germany).....	40
Figure 3. 8.	The DOSE-1 electrometer (Wellhofer Dosimetrie, Schwarzenbruck, Germany).....	41
Figure 3. 9.	The WP1D water phantom and Accessories (IBA Dosimetry GmbH, Germany).....	42
Figure 3. 10.	Blue water Phantom (IBA Dosimetry, GmbH, Schwarzenbruck, Germany).....	43
Figure 3. 11.	Kodak Extended Dose Range 2 (EDR2) film (Carestream Health, Inc, NY, USA).....	44
Figure 3. 12.	Solid water phantom (RMI Gammex, Middleton, WI, USA).....	45
Figure 3. 13.	Vidar VXR16 Dosimetry Pro scanners (Vidar Systems Corporation, Hendon, VA, USA).....	46
Figure 3. 14.	EDR2 film calibration technique.....	51
Figure 4. 1.	Percentage depth dose curve comparisons between eMC calculation and diode detector measurements for standard $10 \times 10 \text{ cm}^2$ field.....	53
Figure 4.2- a.	Measurements of beam profiles in Blue phantom for field sizes of $1 \times 1, 2 \times 2, 3 \times 3, 4 \times 4, 5 \times 5$ and $10 \times 10 \text{ cm}^2$ at 1 cm depth for 6 MeV.....	55
Figure 4.2- b.	Measurements of beam profiles in Blue phantom for field sizes of $1 \times 1, 2 \times 2, 3 \times 3, 4 \times 4, 5 \times 5$ and $10 \times 10 \text{ cm}^2$ at 2 cm depth for 12 MeV.....	56

Figure 4.2- c.	Measurements of beam profiles in Blue phantom for field sizes of 1x1, 2x2, 3x3, 4x4, 5x5 and 10x10 cm ² at 2 cm depth for 20 MeV.....	56
Figure 4.3- a.	Comparisons between calculated and measured beam profiles for cutout 5x5 cm ² for 6MeV.....	57
Figure 4.3- b.	Comparisons between calculated and measured beam profiles for cutout 5x5 cm ² for 12 MeV.....	58
Figure 4.3- c.	Comparisons between calculated and measured beam profiles for cutout 5x5 cm ² for 20 MeV.....	58
Figure 4. 4.	Output factors as a function of side of square field for 6, 12 and 20 MeV	62
Figure 4.5- a.	Output factors of calculation and measurement for cutout sizes from 1x1 to 9x9 cm ² at 6 MeV.....	64
Figure 4.5- b.	Output factors of calculation and measurement for cutout sizes from 1x1 to 9x9 cm ² at 12 MeV.....	65
Figure 4.5- c.	Output factors of calculation and measurement for cutout sizes from 1x1 to 9x9 cm ² at 20 MeV.....	65
Figure 4. 6.	Sensitometric curves of the Kodak EDR2 film for 10x10 cm ² standard cones for a) 6 MeV, b) 12 MeV and c) 20 MeV electron beams	67
Figure 4.7- a.	Isodose comparisons of a 6 MeV beam along the central axis for 4x4 cm ² cutout at 100 cm SSD using 10 × 10 cm ² cone.....	68
Figure 4.7- b.	Isodose comparisons of a 12 MeV beam along the central axis for 4x4 cm ² cutout at 100 cm SSD using 10 × 10 cm ² cone	68
Figure 4.7- c.	Isodose comparisons of a 20 MeV beam along the central axis for 4x4 cm ² cutout at 100 cm SSD using 10 × 10 cm ² cone.....	69
Figure 4. 8.	Gamma analysis results of dose distribution for beams energy of 6, 12 and 20 MeV for cutout sizes of 10x10, 4x4, 3x3, 2x2 and 1x1 cm ²	70
Figure 4.9- a.	Comparison of output factor between calculated and measured for standard and irregular shape of 2 cm at small one side.	73
Figure 4.9- b.	Comparison of output factor between calculated and measured results for standard and irregular shape of 3 cm at small one side.	74

- Figure 4.10- a.** Mean distance discrepancies in PDD (in mm) between calculated and measured dose evaluated at 5% intervals between 20% and 80% dose range for standard and irregular shape of 2 cm at small one side.74
- Figure 4.10- b.** Mean distance discrepancies in PDD (in mm) between calculated and measured dose evaluated at 5% intervals between 20% and 80% dose range for standard and irregular shape of 3 cm at small one side75
- Figure 4.11- a.** Comparison Dose Distribution between calculated and measured results for standard and irregular shape of 2 cm at small one side.75
- Figure 4.11- b.** Comparison Dose Distribution between calculated and measured results for standard and irregular shape of 3 cm at small one side.76

LIST OF ABBREVIATIONS

Abbreviation	Term
a	The accelerator window surface
cGy	Centigray
cm	Centimeter
d_0	The reference depth along the central axis of the electron beam
d_m	Depth of maximum dose
$D_c(r)$	Dose calculation as the compared information at position r
D_d	Dose at the depth d
D_{d_0}	Dose at the reference depth
D_{max}	The maximum dose
$D_m(r)$	Dose measurement as the reference information at position r
D_s	Dose at the surface of phantom
eMC	electron Monte Carlo
E	Energy of electron beam
E_a	The single energy of electron beam
E_m	The maximum energy in an electron beam
$E_{m,z}$	The maximum energy in an electron beam at the depth z
E_p	The most probable energy in an electron beam

\bar{E}	The mean energy in an electron beam
\bar{E}_o, \bar{E}_z	Mean electron energy in an electron beam at the phantom surface and at the depth z
$E_{p,a}; E_{p,o}; E_{p,z}$	The most probable energy in an electron beam at the accelerator exit window, phantom surface and at depth z
FS	Field size of cutout
IAEA	International Atomic Energy Agency
IMRT	Intensity Modulated Radiation Therapy
I_o	The intensity of light incident on a region of the film
I_t	The intensity of light transmitted through the region of the film
IPS	Initial Phase Space model
mm	Millimeter
MCU	Main control unit
MMC	Macro Monte Carlo method
MeV	Mega electron volts
MUs	Monitor Units
o	The phantom surface
OD	Optical density of the film
OF	Output factor
PDD	Percentage depth dose
PDFs	Probability distribution functions

R100	The depth of absorbed dose maximum for electron
R90	The depth where the absorbed dose is 90% of maximum
R80	The depth where the absorbed dose is 80% of maximum
Req	The field radius for the establishment of lateral scatters equilibrium
RW ₅₀	Radiological width
SSD	Source to surface distance
SAD	Source to axis distance
TLD	The thermoluminescent dosimeter
z	The depth of phantom
ΔD_M	Acceptance criteria for dose difference
Δd_M	Acceptance criteria for the distance to agreement
$\gamma(r_m)$	Gamma index at position r of measurements
Γ	The energy spread
δ_2	Penumbra region of profiles
δ_3	Outside central beam axis region
$\delta_{(50-90)}$	Beam -fringe

CHAPTER 1

INTRODUCTION

1.1. Background and Rationale

Electron beams are often used in treating superficial lesions. The irregular nature of individual tumors frequently requires field shapes other than the standard square, rectangular, or circular shapes provided by various applicators. However, almost all of manufacturers have just provided standard fields of cutout such as 6x6, 10x10, 15x15, 20x20, 25x25 cm² but the doctors may require smaller fields than standard one. So, the cutout need to be constructed from lead alloy shielding materials and can be inserted into standard electron cones or placed directly on the patient (Figure 1.1).



Figure 1. 1. Field size of 1x1, 2x2, 3x3, 4x4, 10x10 cm² cutout

For small fields, it is generally observed that the cutout changes the characteristics of the electron beam, as compared to the unblocked beam. The relative output factor, which is the ratio of the maximum dose along the central axis for the field size in question to that for the reference field size, varies with the field size (Figure 1.2-a). The percent depth dose is changed in the small field, this makes the d_{\max} also shift (Figure 1.2-b). The field size dependence of the depth dose and

output factor for any electron beam is negligible until the field dimensions are smaller than the practical range of the electrons in tissue.

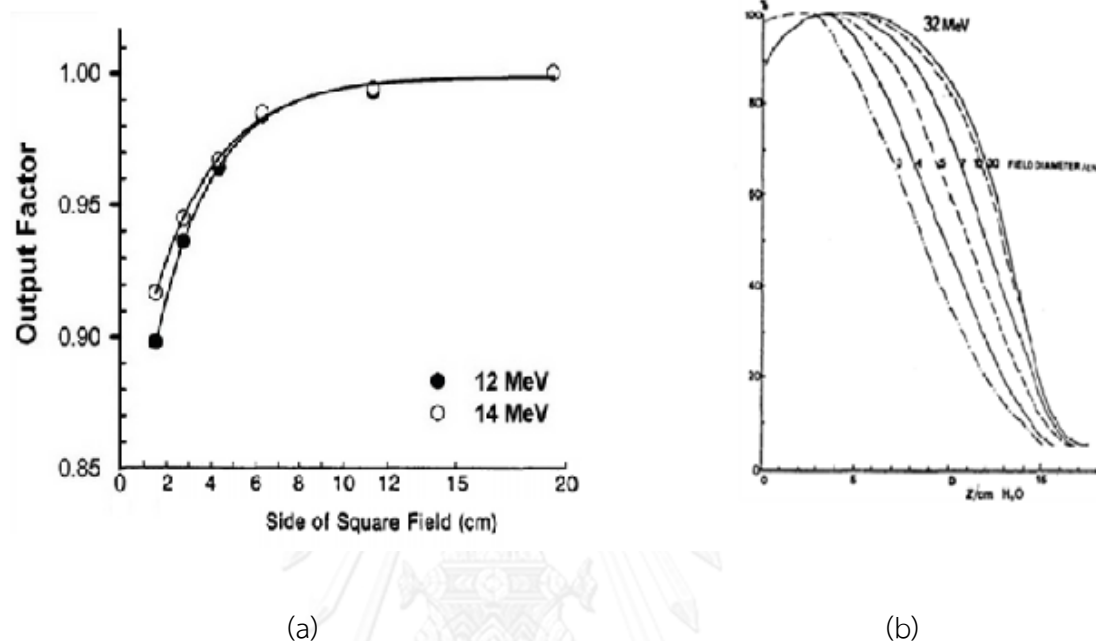


Figure 1. 2. (a) Output factor and (b) Percent depth dose in small field electron beams.

Measurements for the small fields used in clinical practice is the practical difficulties and take long time for set up. Small fields do not exhibit a flat beam profile near the central axis and, therefore, dose measurements with a detector of finite lateral dimensions always show too low average dose compared with the dose at the central axis as shown in Figure 1.3.

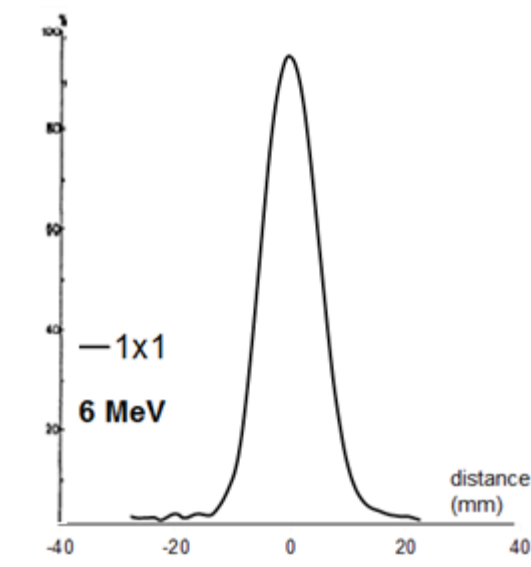


Figure 1. 3. Beam profile of field $1 \times 1 \text{ cm}^2$ electron beams for 6 MeV.

The treatment planning is very important in radiotherapy to calculate dose inside the patient's body. However, output factors for clinical electron beams depend on many parameters. This makes analytical calculation of output factors difficult, especially for small fields. There are several algorithms such as Generalize Gaussian Pencil Beam, Pencil Beam Redefinition Algorithm, Collapse Cone Convolution available for the treatment planning systems to determine the dose distribution and prediction of the electron beam output factors. However, almost of researchers show that the dose calculation accuracy in small field of these algorithms are usually more than 2%.

The construction of small cutouts are necessary for treatment. However, these small fields change the characteristic electron beam due to lack of electronic equilibrium. The accuracy of treatment planning system is very useful. The patient will get the benefit in the dose accuracy, while the physicist has less time for

measurement in all cases. A commercial Monte Carlo based dose calculation algorithm has become available for electron beam treatment planning in the Varian Eclipse treatment planning system. Therefore, this research designs to verify electron Monte Carlo algorithm by comparison of calculations with measurements performed at our institution.

1.2. Research Objectives

The goals of this research work are:

1. To verify dosimetric accuracy of electron Monte Carlo algorithm in Eclipse treatment planning for small field electron beams.
2. To find the minimum size of cutout that electron Monte Carlo algorithm can accurately predict for electron beams.

CHAPTER 2

LITERATURE REVIEWS

2.1. Theories

Electron beams are often used in treating superficial lesions (e.g. skin, lip, chest wall, head and neck cancers) and boosting to nodes, cold spot and blocked areas at the junction of two photon fields with a characteristically sharp drop-off in dose beyond the lesions. Although many of these sites can be treated with superficial x-ray, brachytherapy or tangential photon beams, the electron beam irradiation offers distinct advantages in terms of dose uniformity in the target volume and in minimizing dose to deeper tissues [1].

2.1.1. Energy Parameters of the Electron beam

In an accelerator, the electron beam reaches a specific final energy at the end of its travel through accelerating system. The beam has the maximum energy and the narrowest beam energy spread before passing the exit window. Figure 2.1 shows the electron energies at various points i.e., the accelerator's window surface, the phantom surface and depth in the phantom.

In general, the energy spectrum is characterized by maximum energy E_m , most probable energy E_p , mean energy \bar{E} , and energy spread Γ . Additional subscripts are added to these parameters such as the accelerator's window surface (a), the phantom surface (0) and the depth in the phantom (z).

As illustrated in Figure 2.1, the energy spectrums of an electron beam before passing through the exit window of the accelerator is a narrow peak sufficiently characterized by a single energy value E_a . The most probable energy, $E_{p,a}$ is referred

to the “nominal accelerator energy”. As the electrons beam passes through the exit window, scattering foils, the ionization chamber, and the light mirror shift the electron spectrum to energy lower than $E_{p,a}$ and cause a broaden of the spectrum. At the phantom surface, two energy parameters which are nearly the same value, the “most probable energy” $E_{p,o}$ which is the energy value corresponds the peak of the cure and “mean energy” \bar{E}_o . which is slightly smaller than $E_{p,o}$ by a few MeV. Energy losses from the electron beam are large when the beam traverses the thick layers of the phantom. The beam parameters inside the phantom are the maximum energy $E_{m,z}$, the most probable energy $E_{p,z}$, and the mean energy \bar{E}_z .

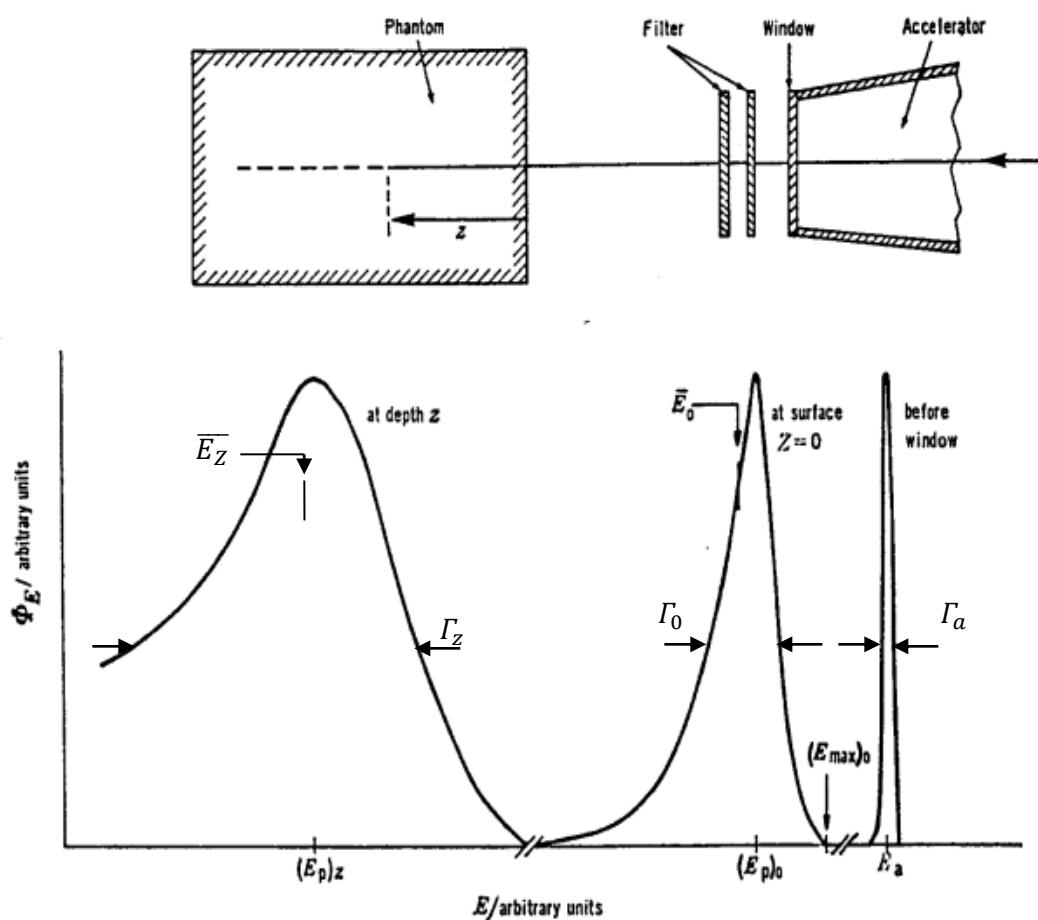


Figure 2. 1. Electron beam energy parameters considered in the accelerator phantom geometry [2].

The Nordic Association of Clinical Physics [3] recommends the specification of most probable energy, $E_{p,o}$ (defined by the position of the spectral peak in Figure 2.1) at the phantom surface and the use of the following relationship:

$$E_{p,o} = C_1 + C_2 R_p + C_3 R_p^2 \quad (2.1)$$

where R_p is the practical range in centimeters. For water, $C_1 = 0.22$ MeV, $C_2 = 1.98$ MeV cm⁻¹, and $C_3 = 0.0025$ MeV cm⁻² [4-6]. They further recommend that the field size for range measurements be no less than 12 x 12 cm² for energies up to 10 MeV and no less than 20 x 20 cm for higher energies.

The mean energy of the electron beam, E_o , at the phantom surface is related to R_{50} (the depth at which the dose is 50% of the maximum dose) by the following relationship:

$$\overline{E}_0 = C_4 R_{50} \quad (2.2)$$

where $C_4 = 2.33$ MeV/cm for water. Again the divergence correction is applied to each point on the depth dose curve before determining R_{50} .

Harder has shown that the most probable energy and, approximately, the mean energy of the spectrum decrease linearly with depth [7]. This can be expressed by the relationships:

$$E_{p,z} = E_{p,o} \left(1 - \frac{z}{R_p} \right) \quad (2.3)$$

and approximately:

$$\overline{E}_z = \overline{E}_0 \left(1 - \frac{z}{R_p} \right) \quad (2.4)$$

where z is the depth.

Equation 2.4 is important in dosimetry because for absorbed dose measurements it is necessary to know the mean electron energy at the location of the chamber.

2.1.2. Physical Characteristics of Electron Beam

2.1.2.1. Percentage Depth Dose (PDD)

As the beam is incident on a patient (or a phantom), the absorbed dose in the patient varies with depth. This variation depends on many conditions: beam energy, depth, field size, distance from source, and beam collimator system. Thus, the calculation of dose in the patient involves considerations in regard to these parameters and others as they affect depth dose distribution. An essential step in the dose calculation system is to establish depth dose variation along the central axis of the beam.

One-way of characterizing the central axis dose distribution is to normalize dose at depth with respect to dose at a reference depth. The quality percentage (or simply percent) depth dose may be defined as the quotient, expressed as a percentage, of absorbed at a fixed reference depth d_o along the central axis of the beam.

Percentage depth dose (*PDD*) is thus:

$$PDD = \frac{D_d}{D_{d_o}} \times 100 \quad (2.5)$$

where d is any depth and d_o is reference depth of maximum dose ($d_o = d_m$).

Parameters are determined from depth absorbed dose distributions as shown in Figure 2.2. An electron beam absorbed dose distribution in a water phantom showing the significance of various parameters: D_m is the maximum absorbed dose, D_x is the absorbed dose due to bremsstrahlung, R_{100} is the depth of dose maximum, R_{85} is the therapeutic range (it is here assumed that $R_t = R_{85}$; the depth at which the therapeutic interval intersects the depth dose curve near the skin entrance is designated by R'_{85}). The practical range R_p and the half-value depth R_{50} are of special importance for range energy measurements: R_p is defined as the depth where the tangent to the descendent part of the curve intersects the prolongation of the bremsstrahlung tail; R_{50} is defined as depth where the absorbed dose is 50% of the maximum.

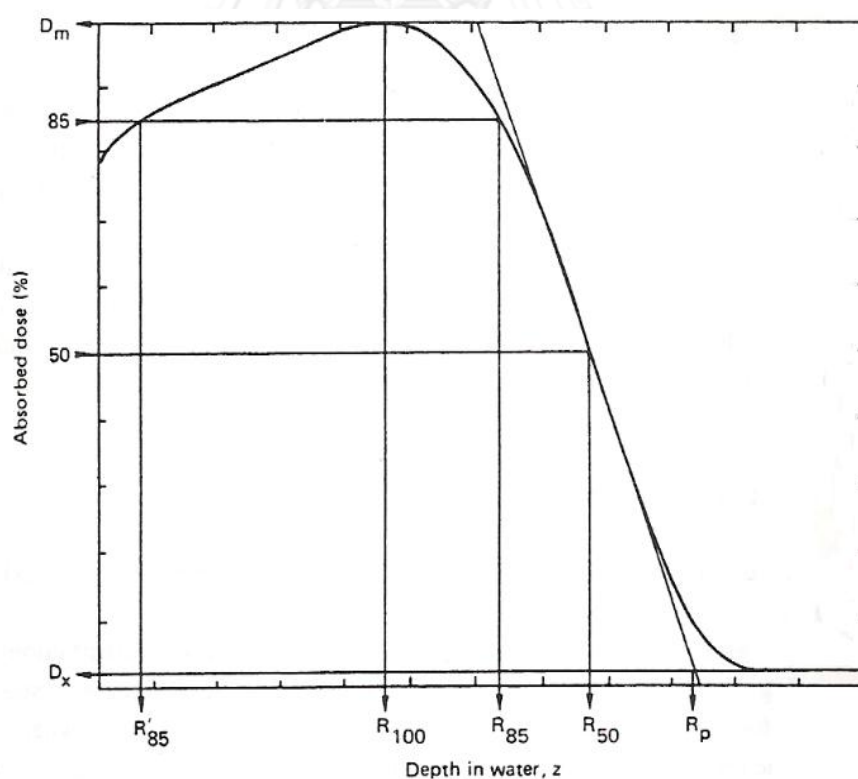


Figure 2. 2. Percentage depth dose curve of electron beam in a water phantom.

The major attraction of the electron beam irradiation is the shape of the depth dose curve, especially in the energy range of 4 to 15 MeV. A region of more or less uniform dose followed by a rapid drop-off of dose offers a distinct clinical advantage over the conventional x-ray modalities. This advantage, however, tends to disappear with increasing energy (Figure 2.3).

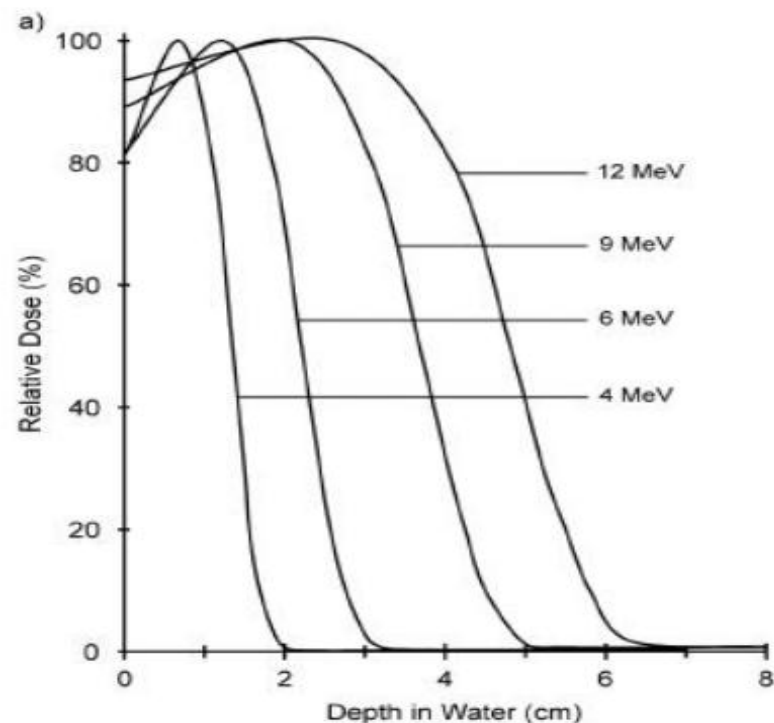


Figure 2. 3. Central axis percent depth dose distribution measured in water for the 4-MeV, 6-MeV, 9-MeV, and 12-MeV electron beams.

2.1.2.2. Beam Profile

Beam profile is a percent dose in a plane perpendicular to the beam axis at a fixed depth. Figure 2.4 shows the dose variation across the field at a specified depth.

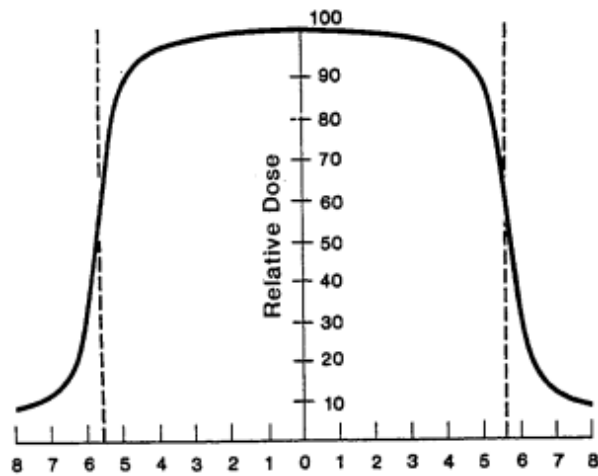


Figure 2. 4. Depth dose profile showed variation of dose across the field.
Dotted line indicates geometric field boundary at a 10 cm depth.

Such a representation of the beam is known as the beam profile. It may be noted that the field size is defined as the lateral distance between the 50% isodose lines at a reference depth. This definition is practically achieved by a procedure called the beam alignment in which the field defining light is made to coincide with the 50% isodose lines of the radiation beam projected on a plane perpendicular to the beam axis and at the standard SSD or source-to-axis distance (SAD).

To compare the beam profiles between measurements and calculations, we can use parameters $\delta_2, \delta_3, \delta_{50-90}, RW_{50}$ showed in Figure 2.5. The required tolerances 2mm for $\delta_2, \delta_{50-90}, RW_{50}$, and 2% for δ_3 were used in this research. The measurements are represented by solid lines while the calculation are represented by dotted lines.

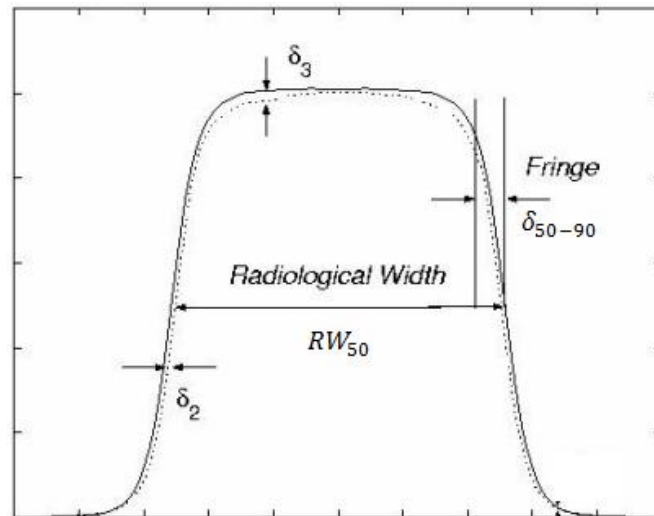


Figure 2. 5. The parameters used to compare beam profiles.

δ_2 - Penumbra region of profiles (High dose, large dose gradient)

δ_3 - Outside central beam axis region (High dose, small dose gradient)

δ_{50-90} - Beam fringe

RW_{50} - Radiological width

2.1.2.3. Output Factor (OF)

The output factors (OF) for any cutout shields are necessary to know accurately to deliver the prescribed dose to the tumor. Output factors for electron beams are defined in this equation.

$$OF = \frac{D_{\max}(E, FS, SSD)}{D_{\max}(E, 10 \times 10 \text{ cm}^2, 100 \text{ cm})} \quad (2.6)$$

where $D_{\max}(E, FS, SSD)$ is the maximum dose on the central axis for a certain beam energy E and the field size FS at a source to surface distance SSD . The factor in the denominator has the same meaning for the reference field, which is taken to be $10 \times 10 \text{ cm}^2$ at 100 cm SSD .

The outputs are highly dependent upon the design of the collimator system, the beam energy and the field dimension. So, the output factors also depend on these factors. The variation of the relative output factor versus field size of the therapeutic electron beam is substantially greater than that produced by high energy photon beam because the dose at d_{\max} of the electron beams is multiple scatters. There is more scattering out of a chamber volume than scattering in the chamber for small field size, so that scattering equilibrium dose not exists. This effect is more significant at low electron energy [8].

2.1.2.4. Isodose Distributions

The central axis depth dose distribution itself is not sufficient to characterize a radiation beam that produces a dose distribution in a three-dimensional volume. In order to represent volumetric or planar variation in absorbed dose, distributions are depicted by means of isodose curves, which are lines passing through points of equal dose (Figure 2.6). The curves are usually drawn at regular intervals of absorbed dose and expressed as a percentage of the dose at a reference point.

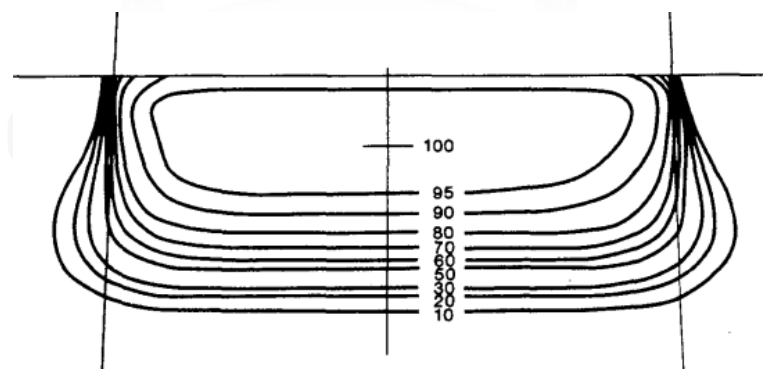


Figure 2. 6. Film used for obtaining isodose curves, exposed to 12 MeV electron beam.

Such a representation of the beam which is known as the beam profile shows the dose variation across the field at a specified depth. Another way of depicting the dose variation across the field is to plot isodose curves in a plane perpendicular to the central axis of the beam (Figure 2.7). Such a representation is useful for treatment planning in which the field sizes are determined on the basis of an isodose curve (e.g., 90%) that adequately covers the target volume.

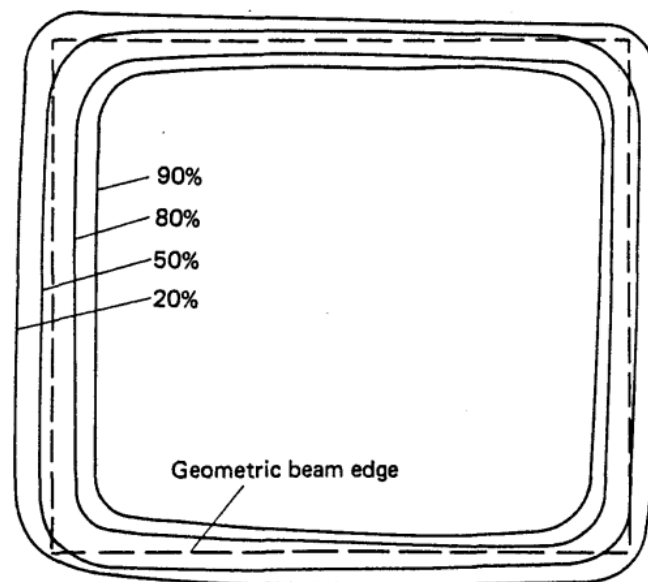


Figure 2. 7. Cross-sectional isodose curves in a plane perpendicular to central axis [9].

Cross-sectional isodose distribution in a plane perpendicular to the central axis of the beam obtained with a film placed in a phantom at the depth of maximum dose. Isodose values are normalized to 100% at the center of the field. The dash line shows the boundary of the geometric field.

2.1.2.5. Shaping the Beam

The electron beams are usually collimated by applicators (cones), which are square beam. However, radiation fields of irregular shape are required and these shapes can be produced by making shield masks or insert cutout, which are placed at the lowest part of a standard cone. The materials frequently used for shielding are lead or a low melting temperature alloy with various trade names such as Cerrobend, Ostalloy 158, MCP-70 and MCP-96. The approximate composition of the first three alloys is 50% bismuth, 27% lead, 13% cadmium and 10% tin with the melting point about 70°C [10]. The last one, MCP-96 that is cadmium free with 90°C melting point consists of 52% bismuth, 30% lead and 18% tin [11]. These alloys are replacing lead as the material of choice for both photon and electron shaping field because of very higher melting of lead with 327°C .

2.1.2.6. Field Size Dependence

The output and the central axis depth dose distribution are field size dependent. The dose increases with field size because of the increased scatter from the collimator and the phantom. As stated previously, some electron collimators provide a fixed jaw opening, and the treatment field size is varied by various cones size, inserts, or movable trimmer bars. Such an arrangement minimizes the variation of collimator scatter, and therefore, the output variation with field size is kept reasonably small. If the collimator aperture (x-ray jaw setting) is allowed to change with the treatment field, the output will vary too widely with field size, especially for lower-energy beams. This effect is shown in Figure 2.8, where the cone size is held fixed while the x-ray jaws are varied. It is noticed that the dose rate varies by a factor of greater than 2 between small and large jaw openings at 4 MeV.

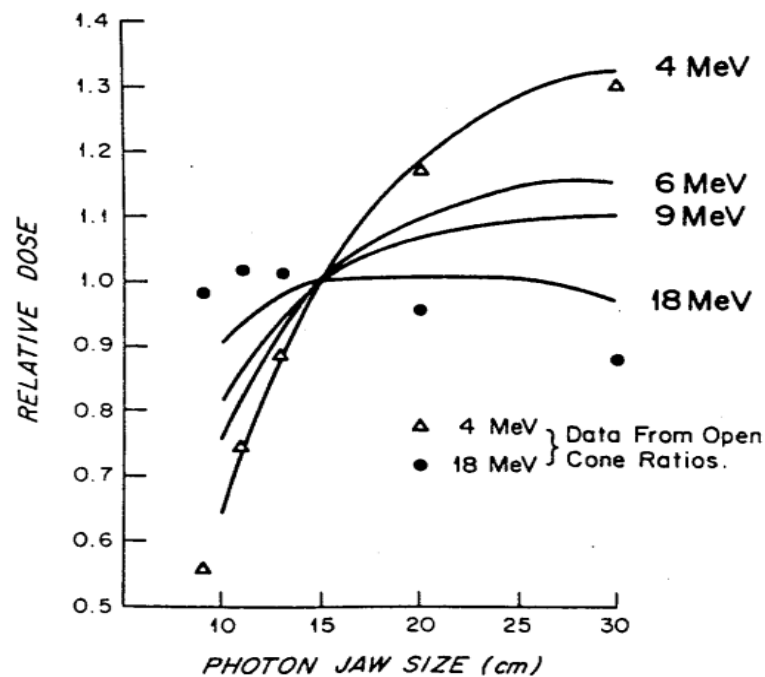


Figure 2. 8. Variation of relative dose at d_m , through a $10 \times 10 \text{ cm}^2$ cone, with the change of jaw setting, relative to the recommended jaw setting [12].

The effects of field size on output and the central axis depth dose curve due to phantom scatter alone is significant as long as the distance between the point of measurement and the edge of the field is shorter than the range of the laterally scattered electrons. When this distance is reached, there is no further increase in depth dose caused by phantom scatter. When the field is reduced below that required for lateral scatter equilibrium, the dose rate decreases rapidly. This is shown in Figure 2.9. In these measurements, the field size at the phantom is varied without changing the cone. For small fields, the output factor as well as depth dose can be significantly reduced compared with the broad beam distribution.

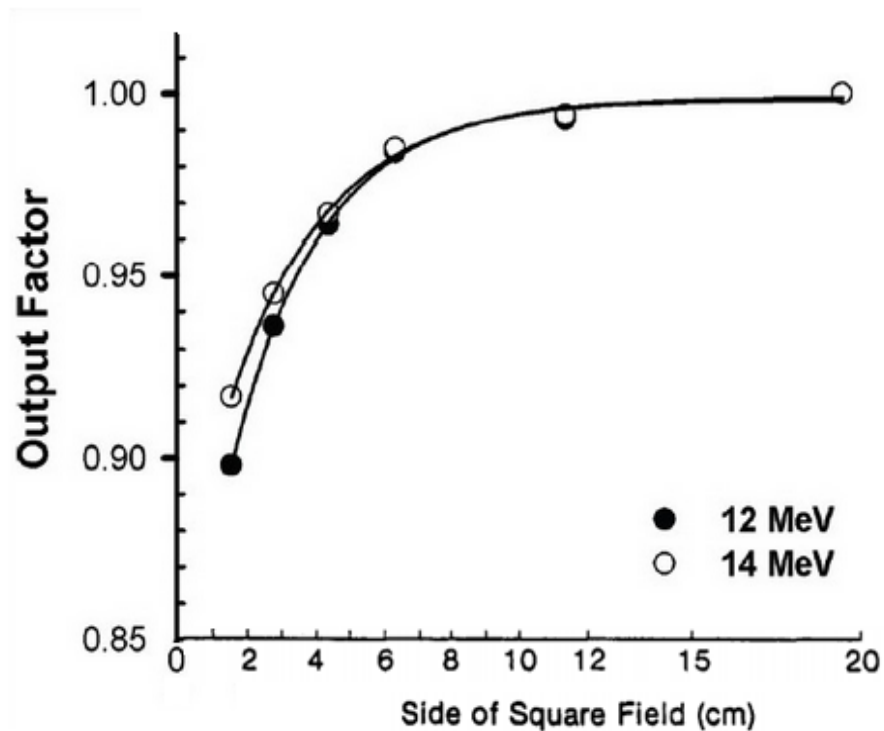


Figure 2.9. Output factors as a function of side of square field. Primary collimator fixed secondary collimators (trimmers) close to the phantom varied to change the field size [13].

Figure 2.10 shows the change in central axis depth dose distribution with field size. As the field size increases, the percent depth dose initially (surface dose, D_s) increases but becomes constant beyond a certain field size when the lateral scatter equilibrium is reached. Furthermore, the depth d_m , R_T and R_{50} shifts toward the surface for the smaller fields, while the R_p is quite constant. Thus in clinical practice, depth dose distribution for small fields should be measured individually in addition to the output calibration.

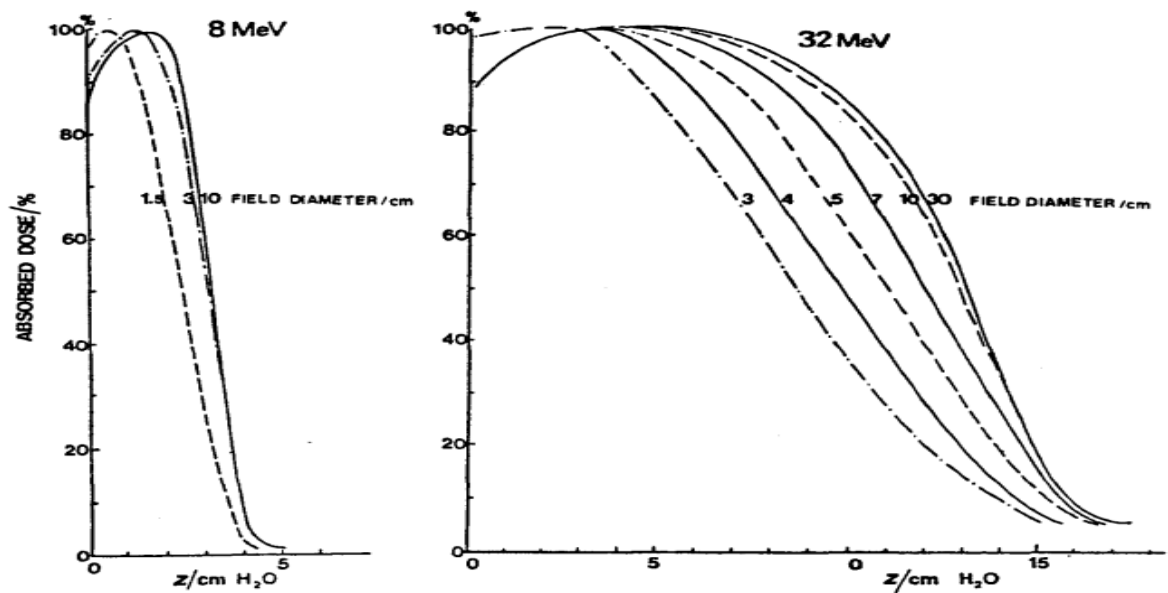


Figure 2. 10. Variation of depth dose distribution with field size of
a) 8 MeV and b) 32 MeV [14]

It has been shown that the minimum field radius for the establishment of lateral scatter equilibrium at all depths on central axis is given by the following approximate relationship:

$$R_{eq} \approx 0.88\sqrt{E_{p,0}} \quad (2.7)$$

where R_{eq} is the field radius in cm and $E_{p,0}$ is the most probable energy in MeV. In clinical practice, the above relationship may be used to classify fields with radius $< R_{eq}$ as small or narrow fields and radius $\geq R_{eq}$, as broad fields. As stated earlier, the depth dose distribution for small fields is field size dependent while broad fields is independent with field size.

2.1.3. Gamma Index Method

The gamma parameter, as presented by Low et al [15], is designed for the comparison of two dose distributions. The method was employed for a comparison between measured and calculated dose distributions in this study. The measurement is used as the reference information ($D_m(r)$), and the calculated distribution is queried for comparison ($D_c(r)$). Figure 2.11 shows a schematic representation of the gamma analysis tool for two dimensional dose distribution evaluations.

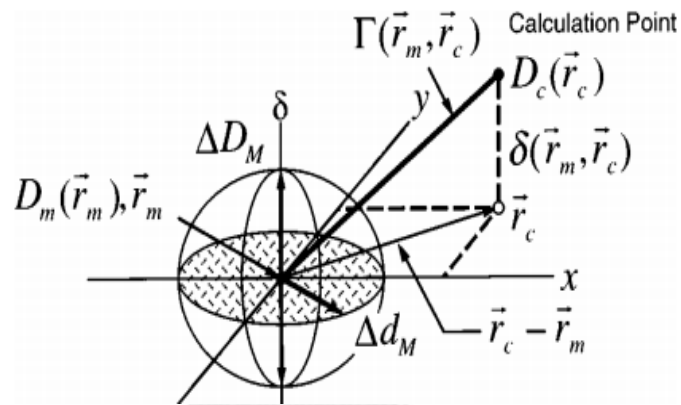


Figure 2. 11. Geometric representation of dose distribution evaluation criteria using the gamma passes technique.

The acceptance criteria are denoted by ΔD_M for the dose difference and Δd_M for the distance to agreement. For a reference point at position r_m , receiving dose $D_m(r_m)$, the surface representing these acceptance criteria is an ellipsoid defined by:

$$1 = \sqrt{\frac{r^2(r_m, r)}{\Delta d_M^2} + \frac{\delta^2(r_m, r)}{\Delta D_M^2}} \quad (2.8)$$

where

$$r(r_m, r) = |r - r_m| \quad (2.9)$$

and

$$\delta(r_m, r) = D(r) - D_m(r_m) \quad (2.10)$$

is the dose difference at the position r_m

If any portion of the $D_c(r_c)$ surface intersects the ellipsoid defined by Eq. (2.8), the calculation passes at r_m .

Defining the acceptance criteria not just along the δ axis and in the $r_c - r_m$ plane allows for a more general comparison between calculation and measurement than does the traditional composite evaluation. The quantity on the right hand side of Eq.(2.8) can be used to identify a quality index γ at each point in the evaluation plane $r_c - r_m$ for the measurement point r_m ,

$$\gamma(r_m) = \sqrt{\frac{r^2(r_m, r)}{\Delta d_M^2} + \frac{\delta^2(r_m, r)}{\Delta D_M^2}}, \quad (2.11)$$

$$r(r_m, r) = |r - r_m| \quad (2.12)$$

and

$$\delta(r_m, r) = D(r) - D_m(r_m) \quad (2.13)$$

is the difference between dose values on the calculated and measured distributions, respectively. The pass-fail criteria therefore become

$\gamma(r_m) \leq 1$, calculation passes,

$\gamma(r_m) > 1$, calculation fails.

An important feature of this method is that in the final assessment of the dose distribution quality, the value of $\gamma(r_m)$ can be displayed in an iso- γ distribution. The

regions where $\gamma(r_m)$ is greater than but nearly unity will be apparent relative to the regions of more significant disagreement.

2.1.4. Electron Dosimeter

The relative measurements determine the spatial beam distribution, whereas absorbed dose requires for absolute methods. At the present time, no single dosimeter is using universal to all of measurement performed in an electron beam. Therefore, to choose a dosimeter that suitable for the purpose and the convenience of measurement are the best advantage. Calorimetric is the most basic method for the determination of absorbed dose, but because of technical difficulties and not practical in a clinical setting, ionization chamber and Fricke dosimeters are more commonly used. Film, thermo luminescent dosimeter (TLD), and solid state diodes are used for the ratio of the dose at one point to another point in a phantom but not usually to measure the absorbed dose at a point. In this study, the silicon diode and film are selected as a relative dose detector.

2.1.4.1. Silicon Diodes

Diode performance depends on the individual detector, regardless of n-type or p-type. Several publications demonstrate that n-type diodes can perform better than p-type diodes [16, 17, and 18].

The electron density of silicon is 18,000 times greater than air. Therefore a silicon diode can be thousands times smaller than an ion chamber, while its sensitivity can still be 10 times higher. The measurement benefit of this is two-fold. First: a higher signal to noise ratio equals better measurement accuracy and reproducibility. Second: a smaller detector equals better measurement precision. Ion

chambers must always be larger than diodes due to their low sensitivity and signal to noise ratio. The silicon diode is a device suitable for scanning because of a very small volume (typically $2.5 \times 2.5 \times 0.4 \text{ mm}^3$) [19]. Therefore, Silicon diode can be used in all field sizes. The small volumes yield high spatial resolution, independence of barometric pressure and recombination effect.

Diode Detector based instruments measure the absolute dose accurately with the dose calibration of the reference detector to the standard accelerator output, exactly as an ion chamber device would do. High sensitivity and good stability give diode detectors an extremely long life expectancy. Life expectancy is at least ten years under normal use. After 100 kGy, diode detectors sensitivity is still much higher than that of an ion chamber.

Diode Detectors exhibit consistent sensitivity with accumulated dose. Sensitivity variation is $<0.5\%/kGy$ at 6MV, $<1.5\%/kGy$ at 10 MeV. The benefit is infrequent calibration ($< \text{once per year}$) even when detectors receive different accumulated doses.

2.1.4.2. Film

Film dosimeter has been used extensively as a convenient and rapid means of measuring dose distributions of therapeutic electron beams in a plane of the film. The data on lateral and depth dose distribution can be obtained in a single exposure. Film also has the property of high spatial resolution and can provide a permanent record of dose distributions in optical density (OD) form. The OD can be defined as

$$OD = \log_{10}(I_o/I_t) \quad (2.14)$$

where I_0 is the intensity of light incident on a region of the film and I_t is the intensity of light transmitted through that region.

A special device, densitometer, measures the degree of blackening on the film in term of optical density. This device has a tiny aperture light source on one side of the film and a light detector (photocell) on the other side of the film to measure the light.

The film is dose rate independent for the range of dose rate found in radiotherapy. In relative dose measurements, the optical density may be taken as proportional to the dose without any correction since the collision stopping power ratio of emulsion to water varies slowly with electron energy. However, film is not good detector for absolute dosimetry because the optical density of the film exposed to electrons depends on many variables such as, emulsion, processing condition, magnitude of absorbed dose. The use of film is recommended to relative dosimetry.

Film can be positioned either perpendicular or parallel to the electron beam axis [20]. Parallel technique film gives a large amount of dosimetric data in a single exposure, while the perpendicular film is less convenient, since many films would need to be taken at various depths to obtain the same amount of data as a parallel film provided.

2.1.5. Electron Monte Carlo Algorithm.

The electron Monte Carlo (eMC) algorithm is a fast implementation of the Monte Carlo method designed for the calculation of the dose distribution from high energy electron beams. The eMC algorithm consists of two models:

- *Initial Phase Space model (IPS)* that describes the electrons and photons emerging from the treatment head of the linear accelerator.
- *Transport model, Macro Monte Carlo (MMC)* method that transports electrons calculating the dose deposited at each point.

2.1.5.1. Initial Phase Space model (IPS).

The IPS consists of 4 sub-sources: a *main diverging source* representing electrons and photons coming from the scattering foil; an *edge source of electrons* which accounts for electrons produced at the edges of the applicator or insert; a *source of transmitted photons* through the applicator or insert and a second *diverging source* which takes into account all the photons and electrons not included in the aforementioned sources. Figure 2.12 shows a schematic view of the 4 sub-sources.

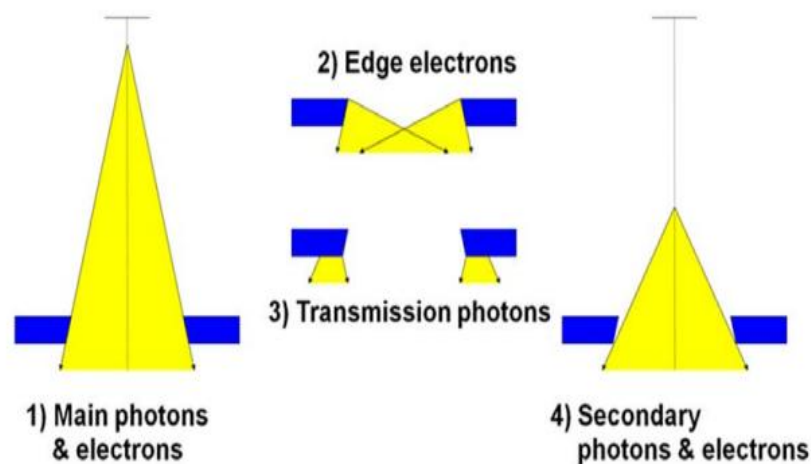


Figure 2. 12. Schematic representation of the four sub-sources used by the IPS model [3]: 1) main photons and electrons, 2) edge electrons, 3) transmission photons and 4) secondary photons and electrons.

Although the cutout material and thickness can be configured in the Beam Configuration task, the eMC algorithm uses the cutout parameters defined in the IPS model for dose calculation. If the cutout material or thickness in use differs from that defined in the IPS model, the calculated dose under the cutout may deviate slightly from the measured dose at the same point, especially when using high energies (18 MeV or higher).

2.1.5.2 Transport model (MMC).

The transport model of the eMC algorithm is the Macro Monte Carlo (MMC) method. Particles are transported through the absorber in macroscopic step based on the probability distribution function (PDFs), which are generated in extensive pre-calculations by employing the EGSnrc code system, generated in the local calculation. Energy deposition is generated by primary and secondary particle transport (Figure 2.13).

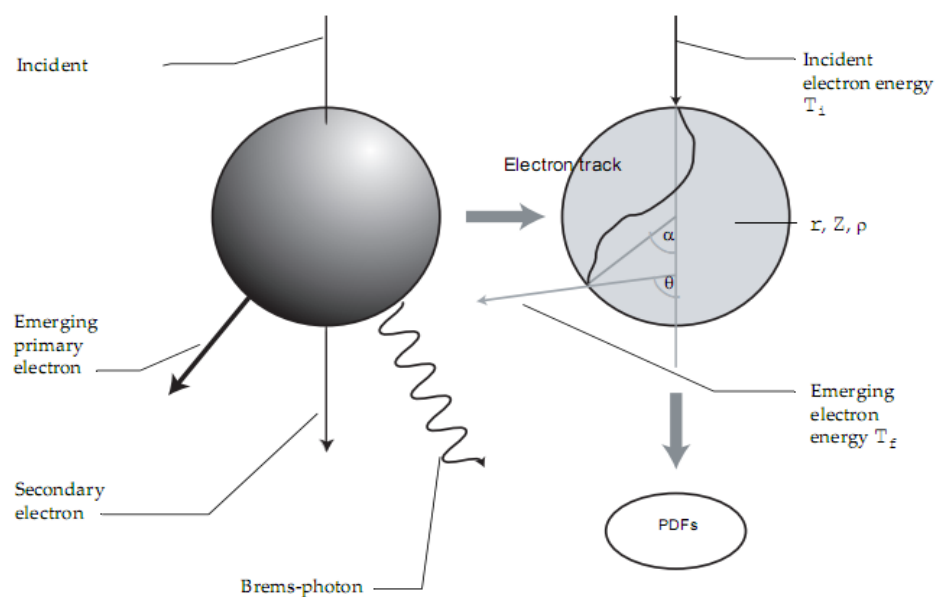
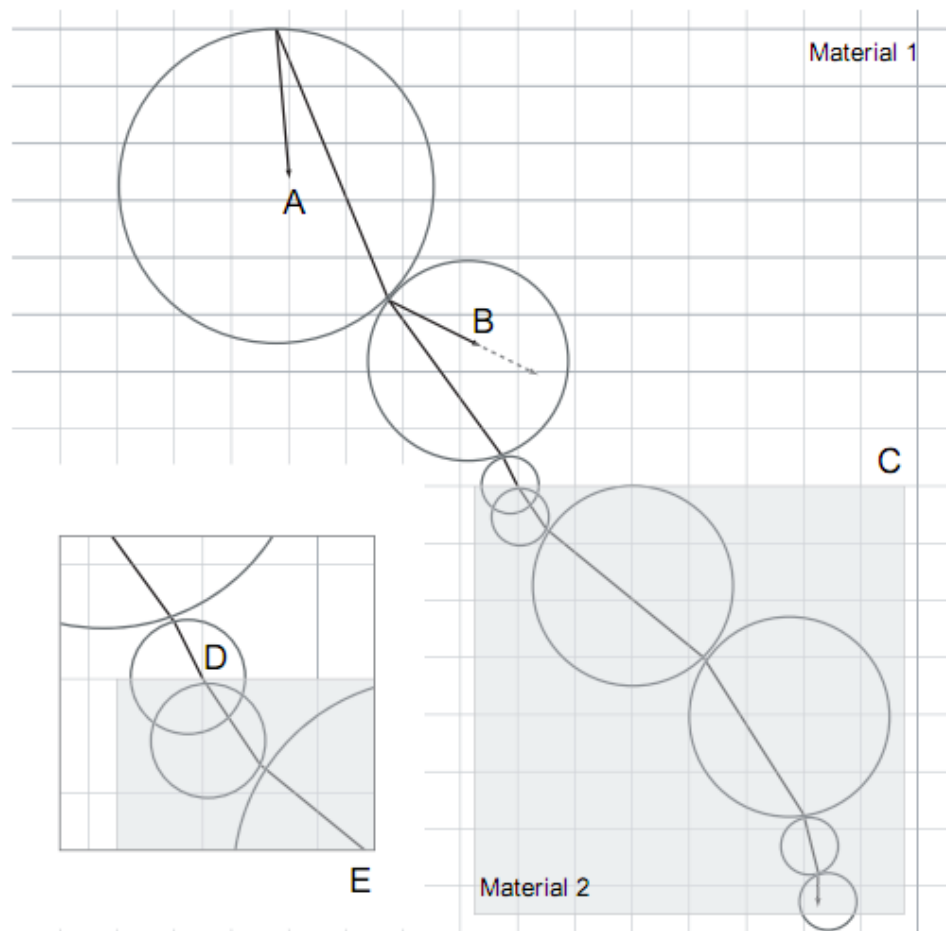


Figure 2. 13. Local geometry used in MMC

For primary electrons, the MMC database contains PDFs for the exit position α , the direction θ and the energy T_f (Figure 2.13) of the emerging primary electron. Figure 2.14 displays a schematic illustration of the primary particle transport algorithm. There is one PDF for each of these parameters for any combination of

- 5 different materials: air, lung phantom, water, lucite, and solid bone phantom
- 5 spheres of radii r : 0.5, 1.0, 1.5, 2.0, 3.0 mm
- 30 incident energy values T_i : 0.2, 0.4, 0.6, 0.8, 1, 1.5, 2, 3, ... 24, 25 MeV



A. Electron direction and step size from previous sphere B. Step size reduction near boundary C. Heterogeneity D. Stop at interface E. Boundary crossing between materials

Figure 2. 14. . Primary electron transport.

For secondary particles (electrons and photons), only the average energy released to these particles per primary electron is stored as a function of the incident primary electron energy T_i in the MMC database. No position or direction parameters are stored for secondary particles. Figure 2.15 presents the secondary particle transport and energy deposition algorithm (the path-length within one voxel has the constant value $\Delta l = D/e$, where D is the dose-grid pitch of the leading Bresenham coordinate and e is the direction cosine for this coordinate).

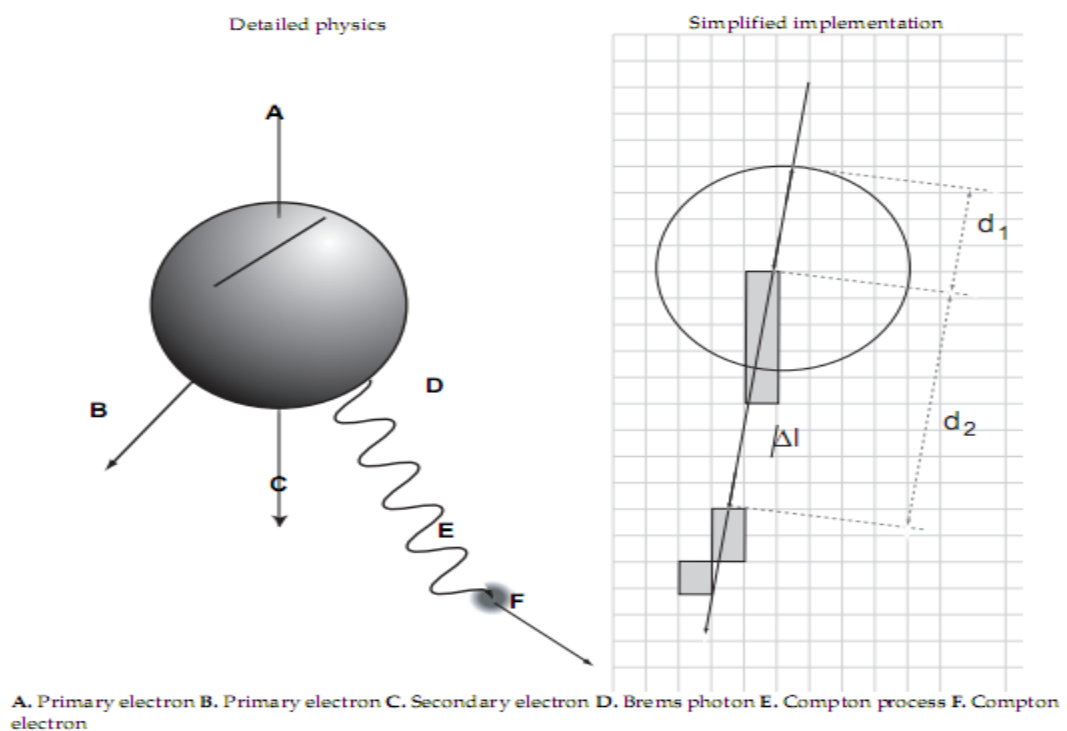


Figure 2. 15. Secondary particle transport

Since there is no information for the position and direction parameters of these particles available from the database, some simplifications have been made in secondary particle scattering and energy deposition.

2.1.5.3. Beam Data Measurements for The eMC Algorithm

The configuration of the eMC algorithm requires beam data measurements for the full open field and energy/applicator combinations.

Open Field Measurements

The following full open-field measurements (without the applicator, with collimator jaws wide open) must be provided for each electron energy level:

- Depth-dose curve in water at the Source-to-Phantom Distance (SPD) = 100 cm
- Absolute dose in water, expressed in [cGy/MU], at the calibration point on the depth dose curve (usually the d_{\max} or a point close to it)
- Profile in air at 95 cm

Energy/Applicator Measurements

For each energy/applicator the following measurements must be provided:

- Relative depth dose curve in water at SSD = 100 cm and absolute dose (in cGy/MU) at the calibration point on the depth dose curve (usually the d_{\max} or a point close to it).

The first point of all depth dose curves must be at the depth of 0.5 mm or shallower.

The beam measurement data must be in the w2CAD format in order to transfer it to the Eclipse Beam Configuration task.

2.1.5.4. eMC Calculation Options

The following calculation options can be configured for calculation models based on the eMC in the Beam Configuration task:

- *Calculation grid size* – Define the resolution of the dose calculation. It can be defined in the External Beam Planning task and Beam Configuration task.
- *Accuracy* - Average statistical uncertainty in the D_{\max} region. The average statistical uncertainty is based on reference calculation, which simulates a 10x10 cm field in a water phantom to the level of $\pm 1\%$ accuracy at the D_{\max} . Increasing the accuracy from 2% to 1% also increases the required amount of particle histories to be simulated, and timer required for completing the simulation, four times.
- *Maximum number of particle history* - Defines the accuracy of the calculation by the amount of particles processed. The 0 value means that this option is not used; instead the Accuracy option is used. The eMC algorithm uses batch of particles in the simulation, each batch consisting of 10,000 particles. The value given for the maximum number of particle history option is always rounded up to the nearest number divisible by 10,000. For instance, if the given value is 10,001 eMC simulates two batches (equaling to 20,000 particles). The number of particles used in the simulation is reported in the dose calculation log.
- *Random generator seed* – Defines the random number sequence used in the particle generator. It can be defined in the External Beam planning task.
- *Smoothing method* – Defines the method of dose distribution smoothing. Possible value are No smoothing, Gaussian and Median.

- *Smoothing levels* – Defines the strength of the dose smoothing. Possible values are Low, Middle and Strong.

2.2. Review of Related Literature

The irregular nature of individual tumors frequently requires shape field other than the standard square, rectangular or circular shapes provide by various cone. Electron fields may be accomplished with the cutouts, constructed from lead or low melting point alloy shielding material (MPC-96 or Cerrobend), to protect non-treatment areas. This would approach to the principles of ideal radiotherapy. The tumor volume should get maximum uniform dose and the surrounding normal tissue should get minimum dose. The used of cutouts will change the characteristics of electron beams especially when the field dimension is smaller than the practical range of electrons in tissue, resulting from scatter electron and bremsstrahlung production by high atomic number cutouts. Therefore, it is necessary to consider individual cutout dosimetry when one field dimension is small. Several theoretical and experimental methods available in literature predicted and determined the characteristics and output factor of electron beams for various linear accelerators.

Rustgi and Working [21] studied the effect of cerrobend cutouts. They measured the central axis depth dose curves, isodose profiles, and output factors at 6-18 MeV electron beams from a Varian Clinac 1800 with ionization chamber, silicon diode detector, and Kodak XV film. Circular fields of 1, 2, 3, 5, and 8 cm in diameter were obtained from cerrobend shields attached to the bottom face of a $15 \times 15 \text{ cm}^2$ electron cone. They founded that the radiation output and depth dose distribution were different from the standard cone due to scatter electrons and bremsstrahlung. As the field size of electron beam becomes smaller; (a) the d_{max} shifts toward the surface, (b) the R_{90} and R_{80} are shallower, (c) the D_s increases, (d) the dose fall off region is less steep, and (e) the R_p remains constant, these effects are also the

function of beam energy. The output was reduced by reduction in electron beam field size as a consequence of lacking of lateral scattered equilibrium. This experiment was confirmed by Shrama et al [22]. They used an ionization chamber, Kodak XV-2film, and TLD-100 chips for measurement.

Recently, most commercial treatment planning systems incorporate electron beam planning programs, however, not all programs have comparable accuracy or limitations. Electron beam dose calculations were originally based on empirical functions that utilized ray line geometries and assumed broad beam dose distributions in homogeneous media [23]. More advanced Pencil Beam algorithms, based on multiple scattering theories, were developed in the early 1980s by Hogstrom et al [24]. One major limitation of both empirical methods and the Pencil Beam algorithms is their inability to predict percentage depth dose distributions and accurate output factor for field sizes smaller than the extent of lateral scatter equilibrium. The approximation for lateral scatter equilibrium was determined by Lax and Brahme to be $\text{Energy}/(\text{MeV})/2.5$ in centimeters of water [25]. The simple algorithm in treatment planning systems cannot accurately predict clinically relevant dosimetric data for cutout diameters less than the Lax and Brahme approximation.

Verhaegen.E [26] evaluated the change of d_{max} in a water phantom for 6 – 20 MeV electron beams of the RMH Varian 2100C linac (SSD = 100 cm) in the small fields from 2 to 7 cm diameter of circular fields and also showed difference of output factors between eMC algorithm and measurement more than 2% in small rectangular fields (3x3, 4x4, 5x5, 6x6, 7x7 cm²). It was due to the large size of a NACP ion chamber to measure small field. Even if the calculated for those small fields agree with the ones measured with an ion chamber with relatively large lateral

dimensions, such as NACP ion chamber, they cannot use as output factors to scale dose in dose distributions. To obtain the appropriate output factors for small fields, they recommended using a small enough dosimeter such that the non-flatness of the dose profile has a small effect on the dose integration.

Zhigang Xu [27] compared eMC calculations and measurements of depth doses, isodose distributions, and monitor units for several different energies 6, 9, 12, 16 and 20 MeV and small field cutout size 5, 4, 3, 2 and 1 cm in water at different SSDs using EBT film (International Specialty Products, Wayne, NJ) and a Pin Point ion chamber (PTW-New York Corp., Hicksville, NY). Their results showed that the Monte Carlo algorithm for electron planning in Eclipse was more accurate than previous algorithms for small field sizes in homogenous mediums. They believed that the minimum cutout size eMC can accurately predict depth doses, isodose distributions, and monitor units for as small as a 3 cm diameter for energies in the 6 to 20 MeV range at 100 cm SSD. When a cutout size or any dimension of a shaped field was smaller than 3.0 cm, calculated dose distribution and MUs can differ significantly from the measurement. At extended SSDs (105–110 cm), the results showed good agreement (within 4%) only for higher energies (12, 16, and 20 MeV) for a field size of 3 cm. As Monte Carlo-based treatment planning systems began to enter clinical practice, one should pay particular attention to those fields with cutout sizes smaller than 3 cm in diameter or at extended SSDs with low energies. In such cases, a special dosimetry (e.g. output factor, depth-dose, and isodose distribution) should be measured and used for the treatment planning.

CHAPTER 3 RESEARCH METHODOLOGY

3.1. Research design

The study is the analytical descriptive study.

3.2. Research design model

First of all, the electron Monte Carlo calculation model in Eclipse treatment planning was employed to simulate the Percent depth dose, output factors, and beam profile and dose distribution of electron beams. After that, these values will be compared with measured values.

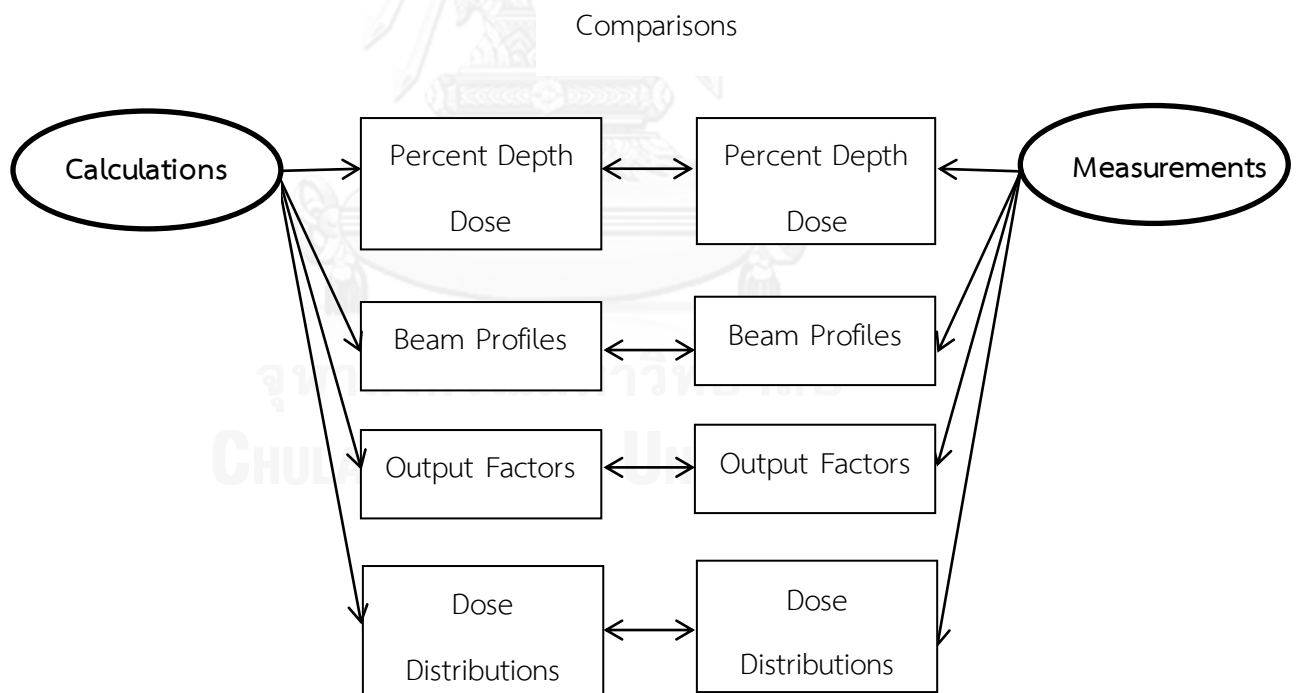


Figure 3. 1. Research design model

3.3. Conceptual framework

In many experiments, they had already shown that the output factors, percentage depth dose, beam profile and dose distribution of electron beams depend on field size, field shaping, SSD, planning algorithm and energy of electron beams (Figure 3.2). However, this study will employed various field sizes and field shaping of cutouts, and energy of electron beams with the fixing of the SSD and planning algorithm.

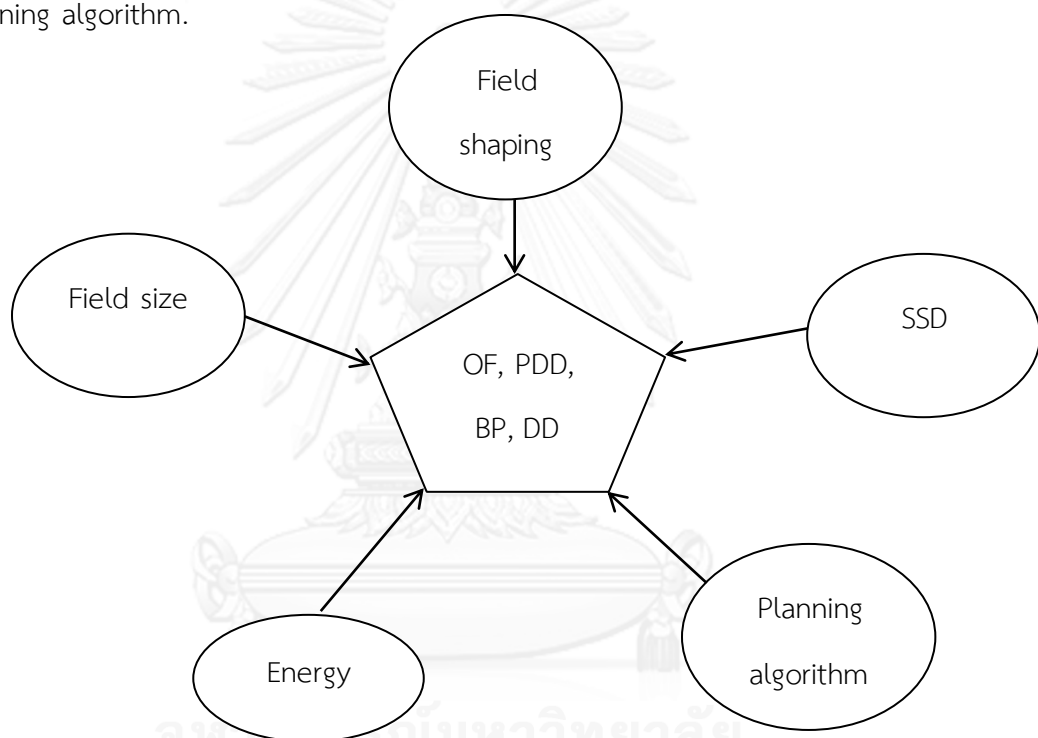


Figure 3. 2. Conceptual framework

3.4. Key word

- Electron beams
- Small fields
- Monte Carlo
- Dose verification
- Treatment planning

3.5. Research Questions

1. What is the dosimetric accuracy of Monte Carlo algorithms in Eclipse treatment planning for small field electron beams ?
2. What is the minimum size of cutout that electron Monte Carlo algorithm can accurately predict for the 6 to 20 MeV energies range at 100 cm SSD ?

3.6 Materials

The materials used in this study included calculation in Eclipse treatment planning system and equipment for measurements such as Linear Accelerator, Cutout Shields, Diode Detector, Electrometer, Phantom, Film and Scanner.

3.6.1. Eclipse treatment planning system

The Eclipse treatment planning system (Varian Medical Systems, Palo Alto, CA) as shown in Figure 3.3 is a comprehensive solution that is open, integrated and easy to use. It opens architecture supports of most treatment modalities and works across numerous linear accelerator platforms. The sophisticated treatment plans can be done with a full palette of powerful tools and robust functionality.

Eclipse allows for treatment planning on a variety of modalities from a single platform, and streamlines the planning process with clinical protocols and templates. It can access all records and dosimetry information from one system including import/export of data with the ARIA oncology information system. Eclipse lets you generate verification plans for IMRT and Rapid Arc applications, as well as perform quality assurance checks. With Eclipse, multiple steps of the treatment planning process come together for greater access and control.

For electron beams, Eclipse treatment planning software, version 8.9.21, can be performed with Generalized Gaussian Pencil Beams and electron Monte Carlo algorithms to calculate dose.

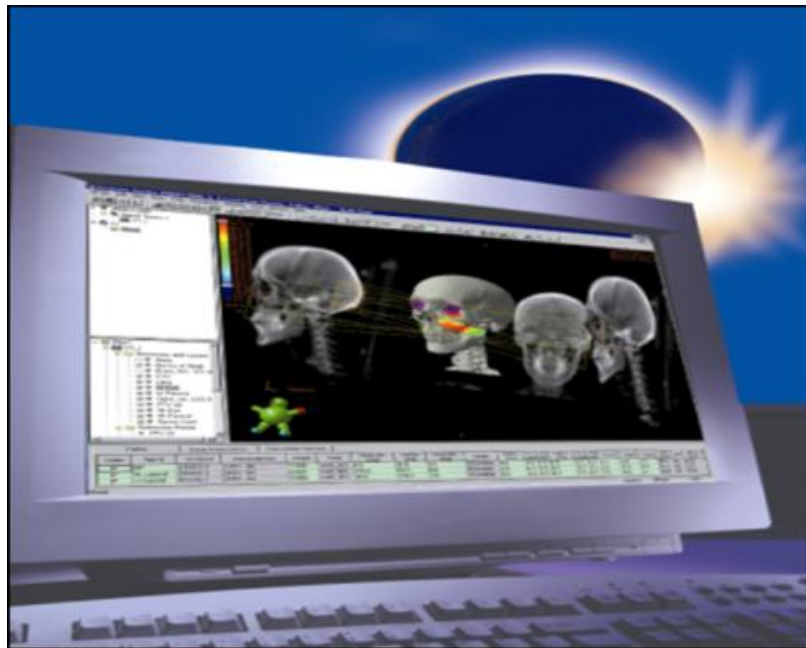


Figure 3. 3. Eclipse treatment planning software (version 8.9.21)

3.6.2. Linear Accelerator

The Varian Clinac iX (Varian Medical Systems, Palo Alto, CA) linear accelerator (Linac) used in the experiment can produce two useful photon beams with the energies of 6 and 10 MV, six useful electron beams with the energies of 4, 6, 9, 12, 16 and 20 MeV. This machine is a standing wave type with dual scattering foils. Photon field sizes are ranged from 0.5x0.5 to 40x40 cm² at 100 cm source to surface distance (SSD), while electron has the standard applicators of 6x6, 10x10, 15x15, 20x20 and 25x25 cm². The adjustable x-ray jaws, which are interlocked to each electron cone, are set automatically larger than the electron field size used. Table

3.1 showed the adjustability of x-ray jaws is symmetrically preset by the manufacture software for each beam energy and electron applicator combination. Stationary therapy dose rate varied from 100 to 600 monitor units per minute are available in six-fixed step. Figure 3.4 displays the linac used in this experiment.

Table 3. 1. The collimator jaws opening (cm^2) for given cone sizes.

Cone size	Energies				
	6 MeV	9 MeV	12 MeV	16 MeV	20 MeV
6x6 cm^2	20.0 x 20.0	20.0 x 20.0	11.0 x 11.0	11.0 x 11.0	11.0 x 11.0
10x10 cm^2	20.0 x 20.0	20.0 x 20.0	14.0 x 14.0	14.0 x 14.0	14.0 x 14.0
15x15 cm^2	20.0 x 20.0	20.0 x 20.0	17.0 x 17.0	17.0 x 17.0	17.0 x 17.0
20x20 cm^2	25.0 x 25.0	25.0 x 25.0	25.0 x 25.0	23.0 x 23.0	22.0 x 22.0
25x25 cm^2	30.0 x 30.0	30.0 x 30.0	30.0 x 30.0	28.0 x 28.0	27.0 x 27.0



Figure 3. 4. Varian Clinac iX linear accelerator

(Varian Medical Systems, Palo Alto, CA)

3.6.3. Cutout Shields

Low-melting point alloy (Lipowitz's metal, MCP-96) cutout, with cadmium free (52% bismuth, 30% lead, and 18% tin) was used for shaping 15 electron fields for $10 \times 10 \text{ cm}^2$ standard cone as shown in Figure 3.5.

- Square fields: from 1×1 to $10 \times 10 \text{ cm}^2$.
- Rectangular fields: 10×1 , 10×2 , 10×3 , $10 \times 4 \text{ cm}^2$
- Circle fields: 1, 2, 3 and 4 cm in diameter.
- L shapes: 1, 2, 3 and 4 cm in width.

These cutout sizes were chosen to study the change of the characteristic of electron beams. Considering that when at least one field dimension is smaller than the practical range of the electron the characteristics of the electron beams are altered.

The $10 \times 10 \text{ cm}^2$ standard cone (Figure 3.6) was chosen because this cone is normally used to treat the patient. The cutouts are designed to fit snugly into the bottom face of $10 \times 10 \text{ cm}^2$ electron cone, so that there is minimal leakage between the face of applicator and cutout. The thickness of the cutout is approximately 1.2 cm for all the electron energies.



Figure 3. 5. The various shape and size of cutout shields insert in a $10 \times 10 \text{ cm}^2$ standard cone.



Figure 3. 6. The 10x10 cm² standard cone of Clinac iX linear accelerator

3.6.4. Diode detector

The field detector-IBA-EFD10025 Electron Dosimetry Diode Detector (IBA Dosimetry GmbH, Germany) and the reference Diode Detectors-EFD10024 (0.015 cm³ active volume, 2 mm active diameter, 5 mm active length) were used in this research (Figure 3.7) because with the small field electron beam, the small detector size during verification is essential for measurements. Diode detectors are the smallest available detector by orders of magnitude. The reference and field detectors are semiconductors. The field detector allows field measurements with high spatial resolution due to small size of the active semiconductor chip (p-type silicon diode, 2.5x2.2x0.54 mm³). The chip can be positioned near the surface since it is 0.57 mm from the front surface of detector. The reference detector is specially designed to achieve a stable reference signal. It is used to eliminate the influence of variations in output from the accelerator.



Figure 3. 7. The Diode Detector– EFD10025
(IBA Dosimetry GmbH, Germany)

3.6.5. Electrometer

The DOSE 1 (Wellhofer Dosimeter, Schwarzenbruck, Germany) as displays in Figure 3.8 is a portable, single channel, high-precision reference class electrometer that significantly exceeds the recommendations of the IEC 60731 and the AAPM ADCL. It combines superior accuracy with an excellent resolution in a wide dynamic range. The electrometer can be used with ionization chambers, semiconductor detectors and diamond probes for measurements of absorbed dose. In combination with radioactive check sources the response stability of the ionization chambers is verified and the cross calibration performed

Dose, dose rate, average dose rate, charge, current and dose per monitor unit are all measured and displayed simultaneously. Up to 40 detector specific data sets can be stored in a sensor library, including physical and geometrical parameters. The units are Gy, Sv, R, rad, rem, C/kg, Ampere (A), and Coulomb (C) at five digit floating point. Many difference types of ionization chamber may be used and many polarizing

voltages can be selected to supply the ionization chamber in used. Bias voltage is $\pm 500\text{V}$, programmable in steps of 1 V.



Figure 3. 8. The DOSE-1 electrometer (Wellhofer Dosimetrie, Schwarzenbruck, Germany)

3.6.6. WP1D water phantom

The WP1D (IBA Dosimetry GmbH, Germany) is one dimensional, stand-alone motorized water phantom for absolute dose measurements according to AAPM TG-51 (lead filter option needed) and IAEA TRS-398 dosimetry protocols (Figure 3.9).

The measurement depth can be adjusted in steps of 0.1-100 mm with the Smart Control Unit (SCU). Up to 8 data sets with each 62 measurement depths can be preset and stored in the SCU. The SCU can be operated from both the treatment room as well as the control room for convenient remote adjustment of the different measurement depths.



Figure 3. 9. The WP1D water phantom and Accessories
(IBA Dosimetry GmbH, Germany)

WP1D Water Phantom has different detector holders for cylindrical and parallel plate chambers are available.

3.6.7. Blue water phantom

The blue phantom 3D beam analyzing system (IBA Dosimetry GmbH, Schwarzenbruck, Germany) is made from acrylic plastic (perspex), having the scanning volume of $480 \times 480 \times 410 \text{ mm}^3$. It is prepared for external control from the OmniPro-Accept 6.4a software (IBA Dosimetry, GmbH, Germany). This phantom can be used for percent depth dose, beam profile with diode detector. The blue phantom is shown in Figure 3.10.



Figure 3. 10. Blue water Phantom
(IBA Dosimetry, GmbH, Schwarzenbruck, Germany)

The blue phantom 3D beam analyzing system comprises of a three dimensional high precision servo mechanism and a Perspex water tank. On the horizontal x-rail, there is a sliding shoe on which detector holders are in all three dimensions for measuring both horizontal and vertical beams.

3.6.8. Kodak Extended Dose Range 2 (EDR2) film

EDR2 (Carestream Health, Inc, NY, USA) is excellent for relative dosimetry (e.g., dose distribution, field uniformity, equipment characterization: field shapes, port openings, MLCs). With appropriate calibration, film may be applicable to absolute dosimetry (e.g., high-dose treatment strategies such as IMRT). It is a very low speed, fine grained film. The silver content of EDR2 film (Figure 3.11) is about one-half that of Kodak XV2 film so the sensitivity of the film is lower. The responsive range dose of EDR2 is excellent from 25 to 400 cGy and the approximate saturation exposure is 700 cGy. The size of film is 10x12 inches.



Figure 3. 11. Kodak Extended Dose Range 2 (EDR2) film
(Carestream Health, Inc, NY, USA)

Exact dose responses are a function of facility dependent factors including processing conditions (processing time, processing temperature, processing equipment, processing chemistry), the density sampling (digitizer equipment and calibration), and exposure monitoring equipment. The exact response relationship should be measured and verified for the local conditions. Many references have discussed methodology for measuring the response of a film [28-31]. The doseresponse of a film should be measured using appropriate amounts of build-up and backscatter material.

Film is superior in terms of higher resolution, which is advantageous for dose distribution verification.

3.6.9. Solid water phantom

The solid water phantom (RMI Gammex, Middleton, WI, USA) used in this experiment is the material compose of epoxy resins and powder control density and

a radiation property, its density is 1.03 g/cm^3 . The physical form is made in square slab of $30 \times 30 \text{ cm}^2$ with the thickness of 0.2, 0.3, 0.5, 1, 2, 3, 4, and 5 cm (Figure 3.12). The solid water phantom material provides the convenience of a solid phantom without the need for correction factors and it is enable to achieve calibration within 1%.



Figure 3. 12. Solid water phantom

(RMI Gammex, Middleton, WI, USA)

3.6.10. Vidar model VXR-16 scanner

The Vidar VXR-16 automatic film scanning densitometer (Vidar Systems Corporation, Hendon, VA, USA) with Scanditronix/ Wellhofer OmniPro™ IMRT software (Figure 3.13) was calibrated with a Kodak step wedge film to define the relationship between the densitometer signal and the net optical density. The film scanner operates with a resolution of 142 dots per inch (0.179 mm/pixel) and a depth of 16 bits. The special step wedge film was delivered from the manufacturer with an optical density range from 0.04 to 3.65. The reference density value for each

step of the step wedge film was entered into the automatic film scanning densitometer and the graph of the signal versus the net optical density was plotted.



Figure 3. 13. Vidar VXR16 Dosimetry Pro scanners
(Vidar Systems Corporation, Hendon, VA, USA)

3.7 Method.

To evaluate the Varian Eclipse electron Monte Carlo (eMC) algorithm performance for small field sizes, calculations of percentage depth doses, beam profiles, output factors and dose distributions were performed for three energies selected at our institution (6, 12 and 20 MeV) in a water equivalent phantom created in Eclipse.

Then the data obtained from calculations were compared to measurement data, which were performed on Varian Clinac iX linear accelerator.

3.7.1 Calculations

Varian Eclipse electron Monte Carlo (eMC) algorithm is a fast implementation of the Monte Carlo method for dose distribution calculation from high energy electron beams in radiotherapy treatment planning. The algorithm consists of:

- Electron transport/dose deposition model (transport model, Macro Monte Carlo method) performing the transport and dose deposition caused by the electrons in the patient
- Electron beam phase-space model (Initial Phase Space model, IPS) describing the electrons that emerge from the treatment head of the linear accelerator

The eMC has six user selectable parameters for individual calculations: calculation grid size, accuracy, maximum number of particle histories, and random number of generator seed, smoothing method, and smoothing level. To attain accurate calculations and consistency within a reasonable amount of time, the eMC calculation parameters used in this study are listed in Table 3.2 that based on research done by Popple et al [32].

Table 3. 2. Eclipse electron Monte Carlo calculation parameters setup.

Parameters	Values
Calculation grid size	2.5 mm (6, 12 and 20 MeV)
Accuracy	1%
Maximum number of particle histories	0 (calculates until desired accuracy goal is reached)
Random generator seed number	1 to 3100000000
Smoothing method	3D Gaussian
Smoothing level	1-Low

The grid size should be approximately one-tenth of the distal fall off distance of the electron depth dose curve (depth from 80% to 20% of the maximum dose) [32]. A typical eMC calculation takes about 2 minutes on a 2.6 GHz CPU for a 5 cm circular cutout (12 MeV) at 100 cm SSD with 1% accuracy and 2.5 mm grid size.

3.7.2. Measurements and Verifications for Square Fields

All measurements were performed with a Varian Clinac iX linear accelerator for percentage depth doses, beam profiles, output factors and dose distributions for square fields of cutout from 1x1 to 10x10 cm² for 6, 12 and 20 MeV.

3.7.2.1. Percentage depth dose

Percentage Depth Dose is percent dose at any depth divide dose at d_{max} . In this research, percentage depth dose were scanned from the depth 6 cm for 6 MeV, 10 cm for 12 MeV, and 14 cm for 20 MeV to the surface of Blue phantom using field Diode Detectors-EFD10025 and reference detector EFD10024 for cutout size from 1x1 to 10x10 cm².

Percentage depth doses of standard shape for small cutout fields as mentioned above were measured in water phantom at 100 cm SSD using 10x10 cm² applicator and compared with calculation by using mean distance discrepancies (in mm) and standard deviation at 5% intervals between 20% and 80% dose range for beams of 6, 12 and 20 MeV energies.

3.7.2.2. Beam profile

Beam profiles were measured with diode detector-EFD10025 as the field detector and diode detector-EFD10024 for a reference detector in Blue phantom

(IBA Advanced Radiotherapy) for field sizes of 1x1, 2x2, 3x3, 4x4, 5x5 and 10x10 cm² at 1cm depth for 6 MeV and 2cm depth for 12 and 20 MeV. Moreover, the special depths R_{100} , R_{90} , R_{50} are also performed for field sizes of 1x1 and 2x2 cm².

All fields were set at the zero gantry angles and the central axis of the beam was perpendicular to the surface of the phantom. The beam profiles were plotted using the basic software of the OmniPro-Accept Software and normalizing doses at the off-axis points to the dose at the central axis.

Then the beam profiles which have the same setup of measurement were created in Eclipse Treatment Planning system and were compared with beam profiles measured with diode at the same depth and field size by using parameters $\delta_2, \delta_3, \delta_{50-90}, RW_{50}$ [33]. The required tolerances 2 mm for $\delta_2, \delta_{50-90}, RW_{50}$, and 2% for δ_3 were used in this research.

3.7.2.3. Output factors

The accuracy of output factors calculations is an important feature of any treatment planning system. The diode detector-EFD10025 was positioned in Blue phantom at the depth of maximum dose, d_{max} , for each cutout sizes and energies determined from percentage depth dose measurements for each cutout size and energy combination at 100 cm SSDs. In this study, output factors were measured for square fields of cutouts from 1x1 to 10x10 cm².

We verified the accuracy of output factors calculations by comparing calculated and measured outputs needed in expected 2% difference for delivering 100 monitor units (MUs) at d_{max} in a water phantom.

Output factors (OF) [34] were calculated using the Eq.4.1

$$OF = \frac{D_{\max}(E, FS, SSD)}{D_{\max}(E, 10 \times 10 \text{ cm}^2, 100 \text{ cm})} \quad (3.1)$$

where $D_{\max}(E, FS, SSD)$ is the maximum dose on the central axis for a certain beam energy E and the field size FS at a source to surface distance SSD . The factor in the denominator has the same meaning for the reference field, which is taken to be $10 \times 10 \text{ cm}^2$ at 100 cm SSD .

3.7.2.4. Dose distribution

In this study, the EDR2 films were selected for dose distribution with Varian Clinac iX linear accelerator, the films were calibrated before performed measurements for each energies level. Figure 3.14 shows the example of 6 MeV for six variable dose regions (labeled 1-6). Dose regions 1-6 received doses of 9.62, 19.23, 48.09, 96.18, 144.27, and 192.35 cGy, respectively. These doses cover the majority of the manufacturer-specified dynamic range for EDR2 film. After that the dose distributions were investigated for cutouts sizes of 1×1 , 2×2 , 3×3 , 4×4 and $10 \times 10 \text{ cm}^2$, insert to standard applicator $10 \times 10 \text{ cm}^2$ with 100 MU delivered dose.

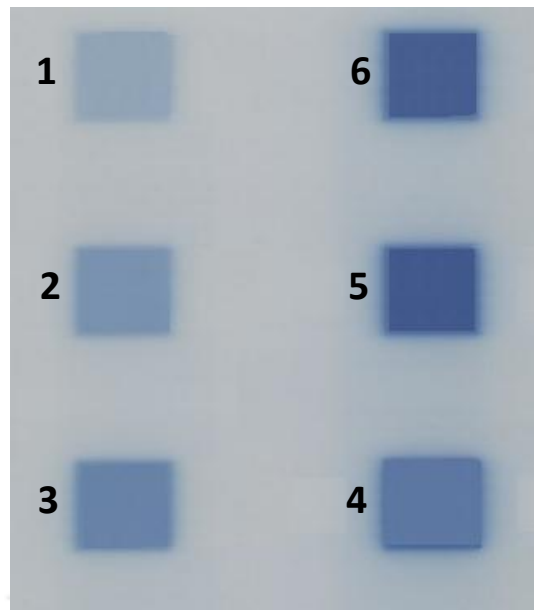


Figure 3. 14. EDR2 film calibration technique.

The EDR2 films were irradiated for each cutout size in solid water phantom with parallel technique. The films were placed at central axis with 100 cm SSD, and sandwiched between solid water phantom slabs.

The optical densities were measured using the film scanner (Vidar model VXR-16 scanner). Dose distributions were plotted as a function of net optical density versus dose for each cutout and energy studied.

Then the dose distribution in each EDR2 films was compared with the calculated dose distribution from Eclipse treatment planning using Scanditronix/Wellhofer OmniPro™ IMRT software by gamma requirements of 2%, 2 mm for all energies tested of Gamma Pass technique.

3.7.3. Measurements and Verifications for Small Irregular Fields

There are not only standard shape of cutouts were studied, but irregular shape as an application in clinical treatments were also performed in this research. Irregular shapes of cutout were made and used in this study for circle, rectangle and L shape, which have the shorter dimension of 1, 2, 3 and 4 cm as showed in Table 3.3.

Table 3. 3. Irregular field shape of cutouts.

Shape Field	Cutout Name	Size of Cutout
Circle	C1	1 cm in diameter
	C2	2 cm in diameter
	C3	3 cm in diameter
	C4	4 cm in diameter
Rectangle	10x1	10 cm in length, 1 cm in width
	10x2	10 cm in length, 2 cm in width
	10x3	10 cm in length, 3 cm in width
	10x4	10 cm in length, 4 cm in width
L shape	L1	1 cm in width
	L2	2 cm in width
	L3	3 cm in width
	L4	4 cm in width

These small irregular fields represent the actual clinical shape. The measurements of percentage depth dose, output factor and dose distribution were set the same as square shapes that have presented above. These values were used to compare with the Eclipse treatment planning calculation and also compare to output of standard shape of cutout in terms of agreements between calculated and measured results of percentage depth dose, output factor and dose distribution for 6, 12 and 20 MeV.

CHAPTER 4

RESULTS AND DISCUSSION

4.1. Square Fields

4.1.1. Percentage Depth Dose

Figure 4.1 shows the comparison between the calculated and measured percentage depth dose curves for 6, 12 and 20 MeV beams for a $10 \times 10 \text{ cm}^2$ open field in water at 100 cm SSD. The eMC calculations are shown as dotted lines and the diode detector measurements are shown as solid lines. The agreement between calculated and measured percentage depth dose for a $10 \times 10 \text{ cm}^2$ open field for all energies were good (within 1 mm) in the linear part of the curve but slightly difference at the build up region and at lower dose and deeper depth.

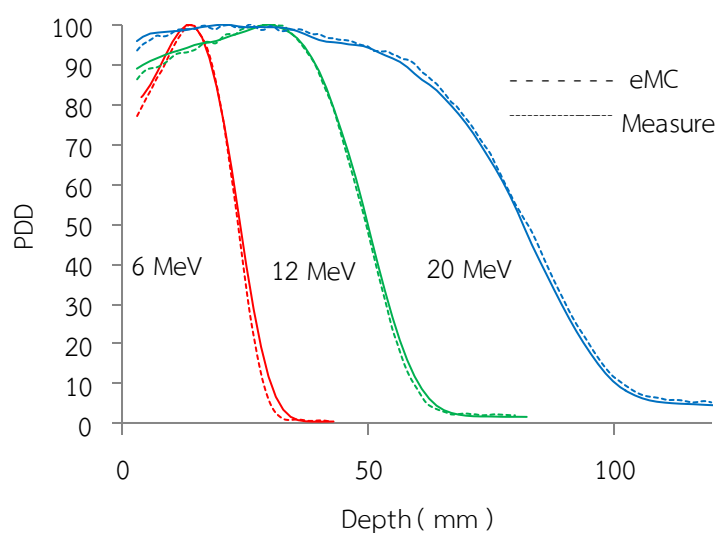


Figure 4. 1. Percentage depth dose curve comparisons between eMC calculation and diode detector measurements for standard $10 \times 10 \text{ cm}^2$ field.

The mean distance discrepancies in percentage depth dose (in mm) and corresponding standard deviations between calculation and measurement doses evaluated at 5% intervals between 20% and 80% dose for 1x1 to 10x10 cm² are given in Table 4.1. The mean distance discrepancies were less than 2 mm, except the 2x2 cm² cutout for 20 MeV that showed 2.1 mm, and the 1x1 cm² cutout showed the largest of 12.8 mm at 20 MeV. The mean difference tended to be increase as the energy increased. These results agreed with Zhigang Xu studied [15].

Table 4. 1. Mean distance discrepancies in PDD (in mm) between calculated and measured dose evaluated at 5% intervals between 20% and 80% dose range for beams of energies 6, 12, and 20 MeV.

Cutout size (cm ²)	Mean distance discrepancies (mm)		
	6 MeV	12 MeV	20 MeV
10x10	0.19±0.12	0.02±0.05	0.38±0.09
9x9	0.02±0.07	-0.20±0.09	-0.43±0.10
8x8	0.09±0.06	-0.25±0.06	-0.53±0.10
7x7	0.41±0.15	0.18±0.09	-0.44±0.04
6x6	0.41±0.10	-0.32±0.13	0.55±0.09
5x5	-0.04±0.07	0.01±0.05	0.58±0.10
4x4	0.39±0.08	0.27±0.05	0.64±0.11
3x3	0.30±0.15	0.48±0.09	0.67±0.15
2x2	1.25±0.12	1.44±0.04	2.11±0.47
1x1	2.26±0.86	7.35±1.27	12.8±2.23

In the high-dose gradient region, the difference between calculated and measured depth doses is never more than 1 mm. The most differences occur at

depths beyond R_{50} . For the high-energy electron beams, the distance from R_{50} to R_p were longer than low energy. The increasing scattered electrons from small cutout combine to long distance from R_{50} to R_p made the percentage depth dose more different in high energies.

4.1.2. Beam Profiles

Beam profiles were measured with diode detector–EFD10025 in Blue phantom for field sizes of 1x1, 2x2, 3x3, 4x4, 5x5 and 10x10 cm^2 at 1cm depth for 6 MeV and 2 cm depth for 12 and 20 MeV. These are shown in figure 4.2(a-c). The X-ray contamination showed the trend of increasing when the energy is increased in both of percentage depth dose and beam profile.

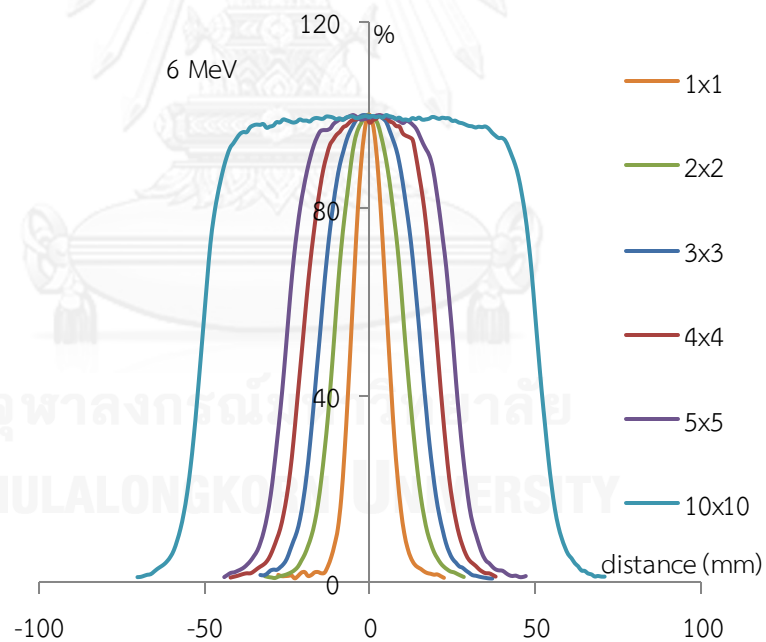


Figure 4.2- a. Measurements of beam profiles in Blue phantom for cutout size of 1x1, 2x2, 3x3, 4x4, 5x5 and 10x10 cm^2 at 1 cm depth for 6 MeV using 10x10 cm^2 cone

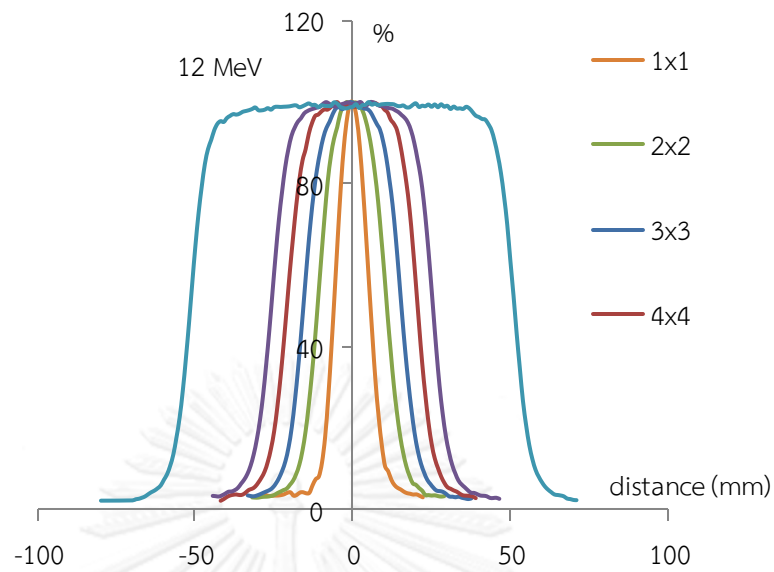


Figure 4.2- b. Measurements of beam profiles in Blue phantom for cutout size of 1x1, 2x2, 3x3, 4x4, 5x5 and 10x10 cm² at 2 cm depth for 12 MeV using 10x10 cm² cone

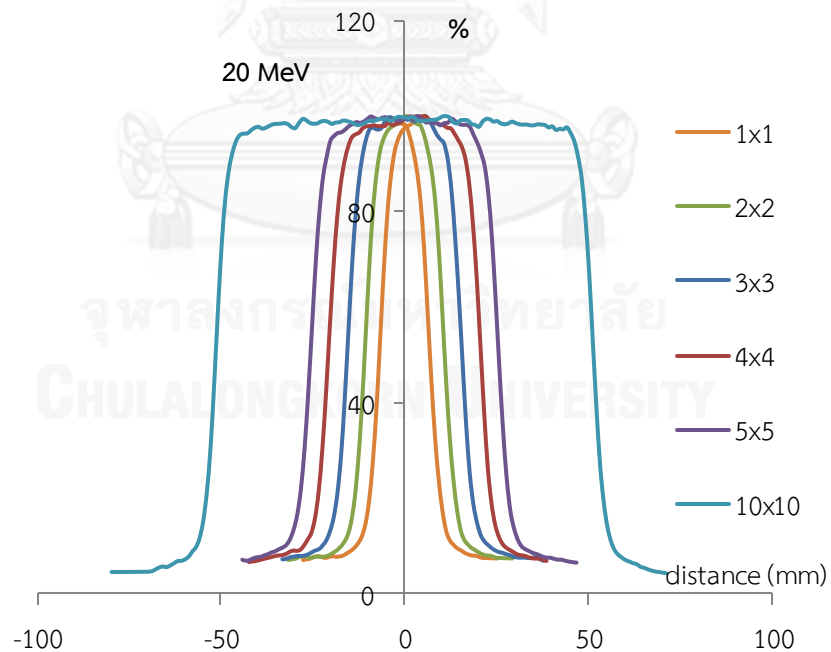


Figure 4.2- c. Measurements of beam profiles in Blue phantom for cutout size of 1x1, 2x2, 3x3, 4x4, 5x5 and 10x10 cm² at 2 cm depth for 20 MeV using 10x10 cm² cone

The comparisons between calculated and measured beam profiles for all of tested energies for cutout of 1x1, 2x2, 3x3, 4x4, 5x5 and 10x10 cm² were illustrated. Figure 4.3(a-c) are examples for cutout of 5x5 cm² for 6, 12 and 20 MeV, respectively. All of the parameters of RW_{50} , δ_2 , δ_3 , δ_{50-90} were within the tolerances which were 2 mm for RW_{50} , δ_2 , δ_3 , δ_{50-90} and 2% for δ_3 parameter as list in Table 4.2(a-c).

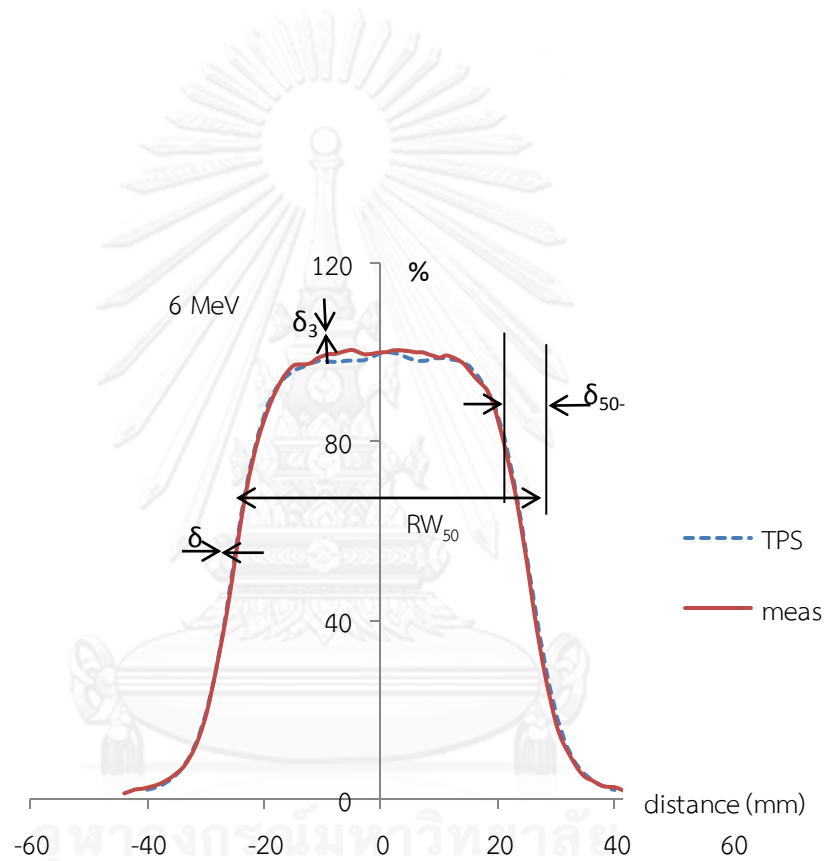


Figure 4.3- a. Comparisons between calculated and measured beam profiles for cutout of 5x5 cm² for 6 MeV at 100 cm SSD using 10x10 cm² cone

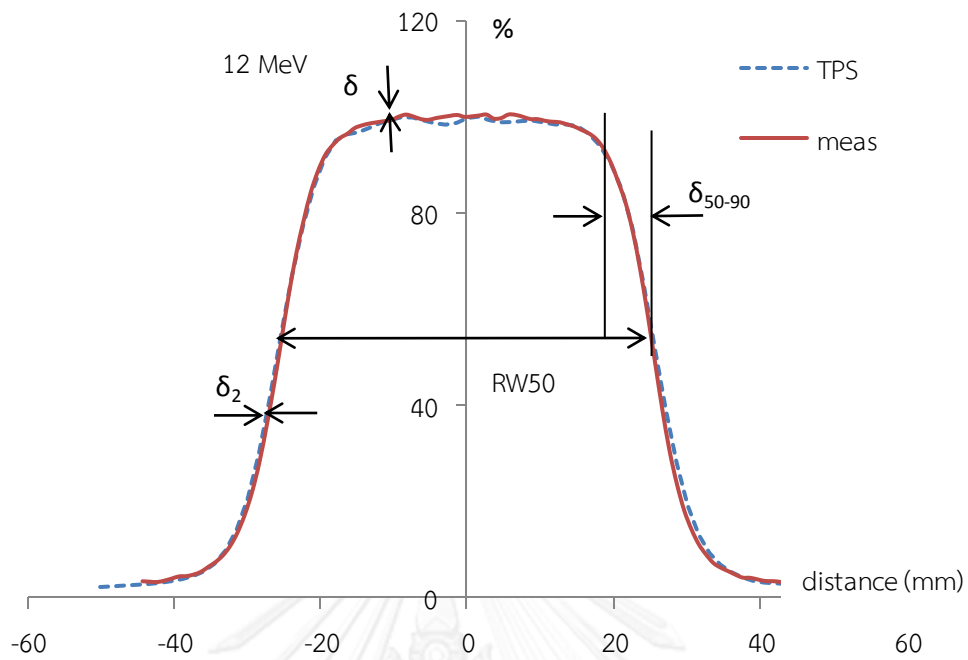


Figure 4.3- b. Comparisons between calculated and measured beam profiles for cutout of $5 \times 5 \text{ cm}^2$ for 12 MeV at 100 cm SSD using $10 \times 10 \text{ cm}^2$ cone

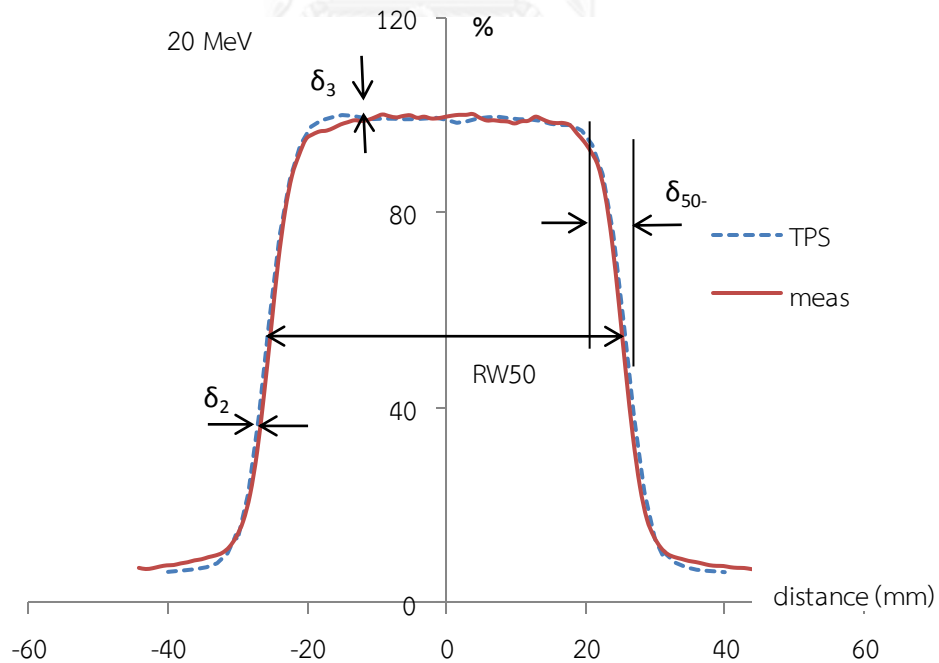


Figure 4.3- c. Comparisons between calculated and measured beam profiles for cutout of $5 \times 5 \text{ cm}^2$ for 20 MeV at 100 cm SSD using $10 \times 10 \text{ cm}^2$ cone

Table 4.2- a. Comparisons of calculated and measured beam profiles for 6 MeV in term of RW_{50} , δ_2 , δ_3 , δ_{50-90} for cutouts of 1x1, 2x2, 3x3, 4x4, 5x5 and 10x10 cm².

Cutout sizes (cm ²)	Depth	RW_{50} (mm)	δ_2 (mm)	δ_3 (%)	δ_{50-90} (mm)
10x10	1 cm	0.35	-0.25	-0.20	-0.17
5x5	1 cm	0.24	-0.02	-0.12	0.11
4x4	1 cm	-0.16	0.04	0.13	0.47
3x3	1 cm	-0.02	0.12	0.11	-0.17
2x2	R100	-0.80	0.37	-0.30	-0.12
	R90	-0.52	0.23	-0.30	0.13
	R50	-1.38	1.05	-0.50	-0.31
1x1	R100	-0.69	0.34	-0.40	-0.22
	R90	-0.46	0.43	-0.27	0.16
	R50	-1.58	1.02	0.61	-0.43

Table 4.2- b. Comparisons of calculated and measured beam profiles for 12 MeV in term of RW_{50} , δ_2 , δ_3 , δ_{50-90} for cutouts of 1x1, 2x2, 3x3, 4x4, 5x5 and 10x10 cm².

Cutout sizes (cm ²)	Depth	RW_{50} (mm)	δ_2 (mm)	δ_3 (%)	δ_{50-90} (mm)
10x10	2 cm	0.55	-0.66	-0.2	0.73
5x5	2 cm	0.51	-0.31	-0.12	0.32
4x4	2 cm	0.06	-0.09	-0.70	0.53
3x3	2 cm	0.30	-0.23	-0.21	-0.33
2x2	R100	0.79	-0.48	-0.51	0.55
	R90	0.37	-0.25	-0.90	0.45
	R50	-1.19	0.52	-0.72	1.65
1x1	R100	0.87	-0.53	-0.41	0.59
	R90	0.34	-0.24	-0.96	0.47
	R50	1.24	0.57	-0.77	1.42

Table 4.2- c. Comparisons of calculated and measured beam profiles for 20 MeV in term of RW_{50} , δ_2 , δ_3 , δ_{50-90} for cutouts of 1x1, 2x2, 3x3, 4x4, 5x5 and 10x10 cm².

Cutout sizes (cm ²)	Depth	RW_{50} (mm)	δ_2 (mm)	δ_3 (%)	δ_{50-90} (mm)
10x10	2 cm	0.56	-0.66	-0.30	0.89
5x5	2 cm	0.86	-0.44	0.21	0.19
4x4	2 cm	0.23	-0.02	0.03	0.02
3x3	2 cm	0.13	-0.14	-0.60	0.12
2x2	R100	0.50	-0.47	-0.20	0.98
	R90	1.33	-1.00	1.20	0.02
	R50	-0.82	-1.23	-0.80	-1.58
1x1	R100	0.61	-0.52	0.27	0.95
	R90	1.41	-1.03	1.25	0.12
	R50	-0.87	1.33	-0.86	-1.79

The results for electron energies of 6, 12 and 20 MeV showed a good match between calculations and measurements. The differences for points at the dose plateau, presented by δ_3 , were usually within 1% and the differences in penumbra which presented by δ_2 is never worse than 1 mm. The lateral beam profiles were also measured and calculated at R_{50} for 1x1 and 2x2 cm² cutout. These results showed slightly deviation than at d_{max} (R_{100}), but never worse than 2 mm.

In general we found that a highly precise model is required for the geometry and composition, especially in the scattering foils, the applicator scrapers, and the cutouts in order to match the calculated and measured depth and lateral dose distributions.

4.1.3. Output factors

The measurements and eMC calculations of output factors for 6, 12 and 20 MeV are shown in Table 4.3, and Figure 4.4 presents the curves of measurements of output factor for 6, 12 and 20 MeV. In these measurements, the field size at the phantom was varied by cutouts from 1x1 to 9x9 cm² without changing the cone. The output factors of large field cutout were not significantly different when varying energies. For small fields, the output factors were significantly reduced compared with the broad beam distribution.

Table 4. 3. Measurement of output factors for 6, 12 and 20 MeV for square fields of cutout from 1x1 to 9x9 cm².

Cutouts (cm ²)	Output Factors					
	Measurements			eMC Calculations		
	6 MeV	12 MeV	20 MeV	6 MeV	12 MeV	20 MeV
1x1	0.62	0.86	0.95	0.72	0.93	1.01
2x2	0.87	0.93	0.98	0.91	0.97	1.00
3x3	0.95	0.96	0.99	0.97	0.97	0.99
4x4	0.98	0.97	1.00	1.00	0.97	1.09
5x5	0.99	0.98	0.99	1.00	0.97	0.97
6x6	0.99	0.99	0.99	1.00	1.00	0.97
7x7	0.99	1.00	0.99	0.98	1.01	0.98
8x8	1.00	1.00	0.99	0.99	1.00	0.98
9x9	0.99	1.00	0.99	0.98	1.01	0.98

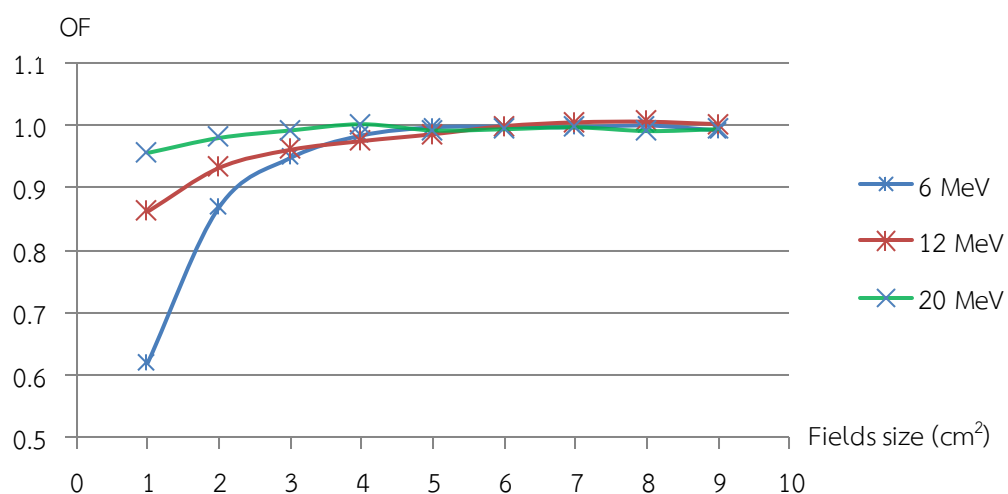


Figure 4. 4. Output factors as a function of side of square field for 6, 12 and 20 MeV

The theory recognizes that all doses in electron beams arise from scattered electrons, which are responsible for the variation of machine output with field size. This variation is customarily expressed as an output factor, defined as the ratio of maximum dose output on the central axis of the field of interest to that of a reference field size. The amount of scattering will depend greatly on the configuration of the collimation system. This accounts for the markedly different output characteristics of machines operating at the same energy, but with different philosophies of design regarding the electron collimation. The amount of scattering is also field size dependent, particularly for the small field sizes, because there is more scattering out of the volume element at d_{\max} along the central axis than into the volume element. This effect is expected to be greatest for the lower energies

because of the higher scattering powers that result in greater lateral spreading of the beam.

The comparison of calculated and measured output factors for beams energy of 6, 12 and 20 MeV and cutout sizes from 1x1 to 10x10 cm² are displayed in figure 4.5(a-c), while the percentage differences using equation $100 \times (D_{cal} - D_{meas})/D_{meas}$ as percentage depth dose and beam profile used for percentage difference dose are shown in Table 5.5. The agreement of output factors were very good (within 2 %) for cutout sizes from 3x3 to 10x10 cm² for all selected energies, except 3x3 cm² which was fairly good within 2.5 % for 6 MeV. For the 2x2 cm² cutout, the calculated output factor was comparable to measurements within 5.1% for all selected energies. These values agreed with ZhigangXu who presented 2.4% for 3x3 cm² at 20MeV and the largest 4.7% for 2x2 cm² [20]. The 1x1 cm² cutout presented the worst results with percent differences 16.4% for 6 MeV.

The output factors from measurements remained significantly lower than the predicted one of the eMC simulations (Figure 5.5-a, b, c) or small fields. The difference exceeds 2% for the case of 2x2 and 1x1 cm², especially for low energy. For 2x2 or 1x1 cutout which is normally small, the positioning of the detector becomes very critical due to the nonflatness of the lateral dose profiles. To obtain the appropriate output factors for small fields, one should use a small enough dosimeter such that the nonflatness of the dose profile has a small effect on the dose integration. Alternatively, Monte Carlo simulations with small enough scoring voxels can be used. However, one should not overlook the fact that the voxels dose in a treatment plan also have finite dimensions. Ideally, the dimension of the

detector or the size of the scoring voxels in Monte Carlo simulations that are used to obtain the output factors should be closely matched the dimensions of the voxels in the treatment planning system.

From Table 4.4, it is obvious that the 6 MeV beam has the largest differences due to the accuracy of chamber positioning. The 6 MeV with small field size has very sharp gradient dose around the d_{max} . Therefore, the accuracy of setting up detector at the central axis beam is required. An initially incorrect positioning led to significant differences between measured and calculated output factors.

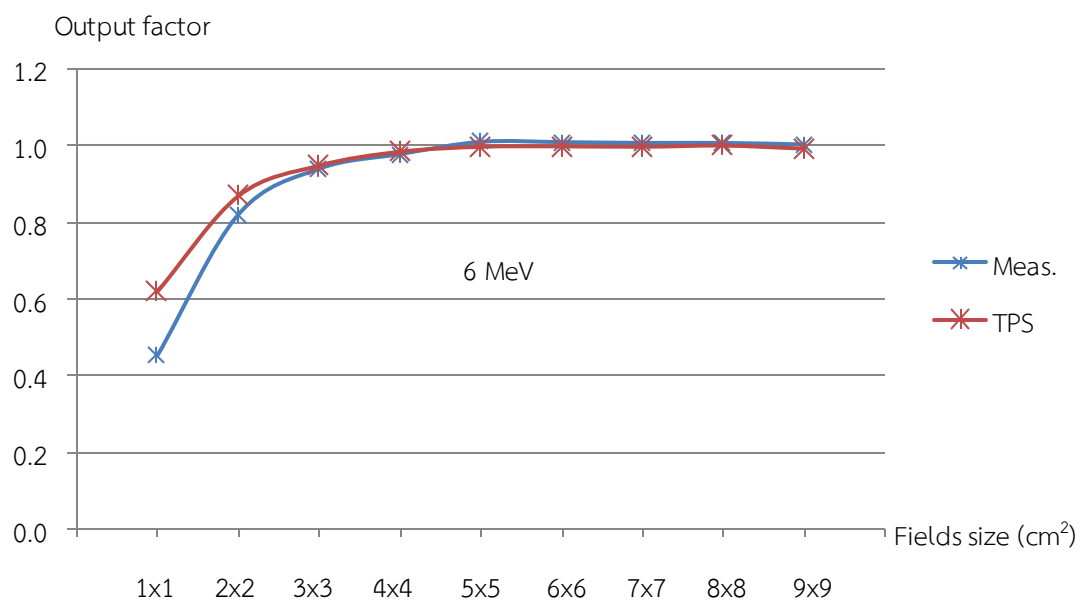


Figure 4.5- a. Output factors of calculation and measurement for cutout sizes from 1x1 to 9x9 cm² at 6 MeV

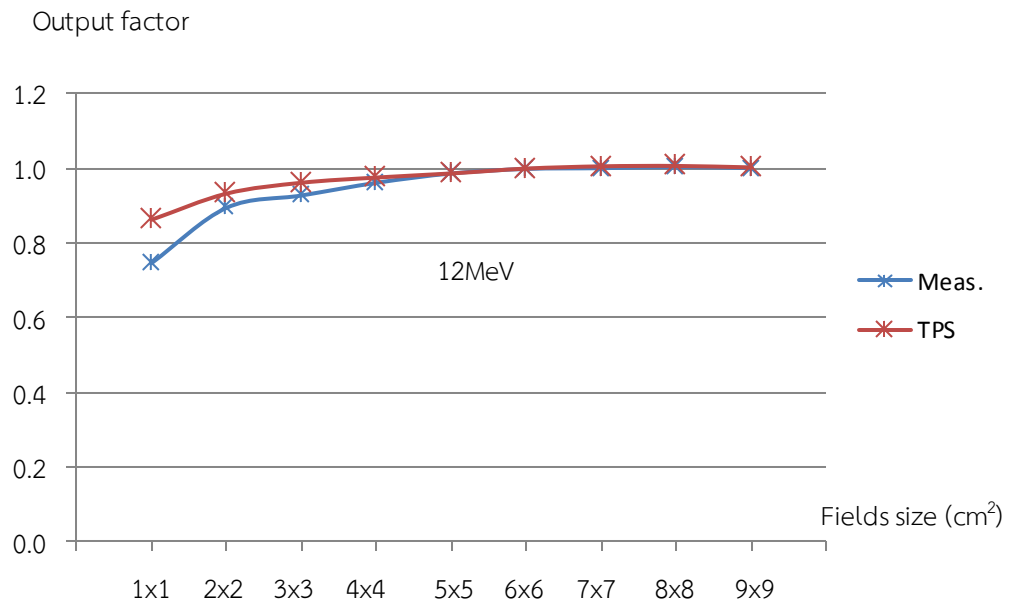


Figure 4.5- b. Output factors of calculation and measurement for cutout sizes from 1x1 to 9x9 cm² at 12 MeV

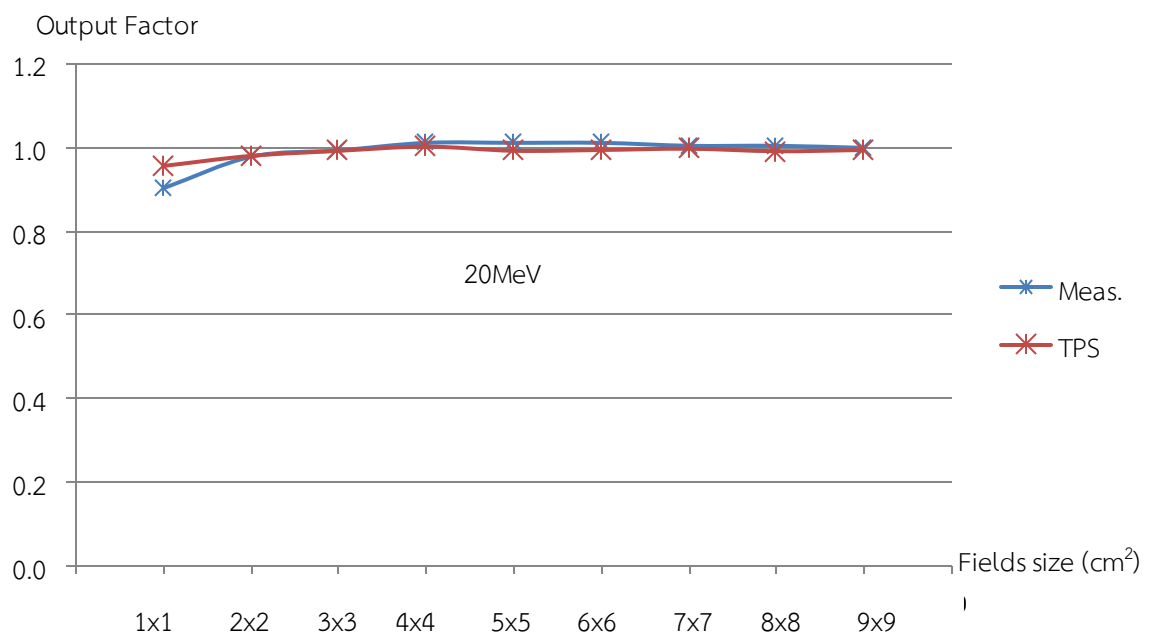


Figure 4.5- c. Output factors of calculation and measurement for cutout sizes from 1x1 to 9x9 cm² at 20 MeV

Table 4. 4. Percentage output factors differences between calculated and measured for cutout sizes from 1x1 to 9x9 cm²

Cutout sizes (cm ²)	Percent output factors differences		
	6 MeV	12 MeV	20 MeV
9x9	-1.1	1.3	-0.6
8x8	-0.7	0.3	-1.3
7x7	-1.0	0.5	-0.7
6x6	0.9	1.2	-1.6
5x5	0.8	-0.6	-1.9
4x4	1.6	0.4	0.9
3x3	2.5	1.5	0.2
2x2	5.1	4.2	2.2
1x1	16.4	7.6	5.8

These results showed the limit of electron Monte Carlo calculation in term of electron scattering and effect of electronic equilibrium. Therefore, these limits make the results of calculation significantly different to measurement in small field of cutout.

4.1.4. Dose distributions

The isodose distributions were measured by EDR2 film. The films should be calibrated for each energy level before performing measurements. The optical density of EDR2 film which perpendicular irradiated as a function of dose for 10x10 cm² cone at electron energy of 6, 12 and 20 MeV are shown in term of the sensitometric curves in Figure 4.6.

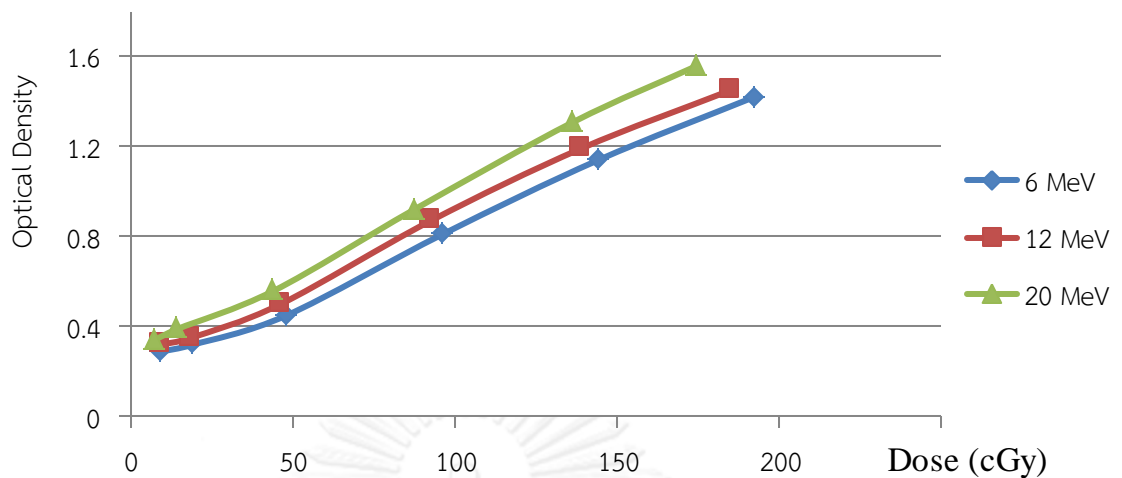


Figure 4. 6. Sensitometric curves of the Kodak EDR2 film for 10x10 cm² standard cones for a) 6 MeV, b) 12 MeV and c) 20 MeV electron beams

The isodose distributions and gamma analysis showed similar result to the depth doses comparisons. A typical isodose distribution for 6, 12 and 20 MeV for cutout size of 4x4 cm² at 100 cm SSD using 10x10 cm² cone were the examples and are shown in Figure 4.7(a-c), thick lines represent eMC calculations and thin lines represent EDR2 film measurements. The 90%, 70%, 50% and 30% isodose lines were selected to compare. Similar results were obtained for other beams of energy and cutout sizes. All comparisons matched well as the values of gamma index represented in Table 4.5. Gamma analysis results for all energies and cutout sizes are shown in Figure 4.8. The agreement between measured and calculated values was excellent for the 10x10, 4x4, 3x3 and 2x2 cm² cutouts, with greater than 92.5% of pixels passing our gamma requirements (2%; 2mm) for all energies tested [20]. The 1x1 cm² cutout showed poor results; the numbers of pixels passing our gamma requirements were below 90% for all the energies tested.

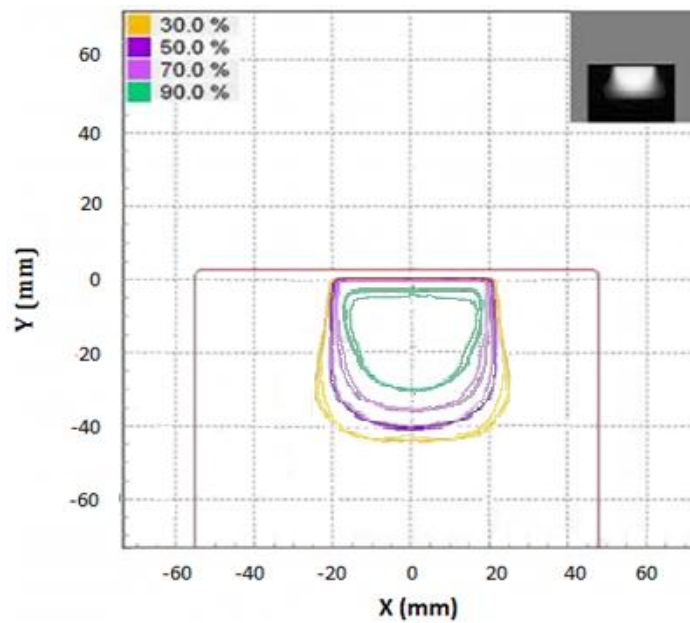


Figure 4.7- a. Isodose comparisons of a 6 MeV beam along the central axis for $4 \times 4 \text{ cm}^2$ cutout at 100 cm SSD using $10 \times 10 \text{ cm}^2$ cone.

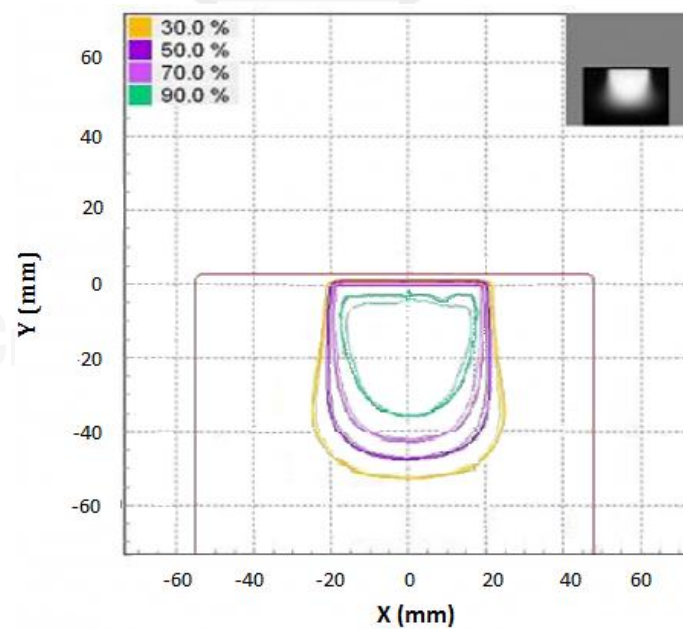


Figure 4.7- b. Isodose comparisons of a 12 MeV beam along the central axis for $4 \times 4 \text{ cm}^2$ cutout at 100 cm SSD using $10 \times 10 \text{ cm}^2$ cone

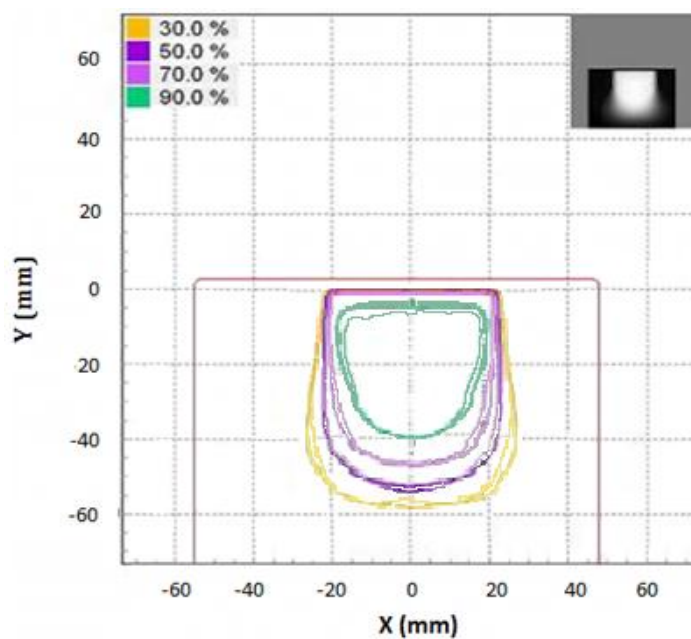


Figure 4.7- c. Isodose comparisons of a 20 MeV beam along the central axis for $4 \times 4 \text{ cm}^2$ cutout at 100 cm SSD using $10 \times 10 \text{ cm}^2$ cone..

Table 4. 5. Gamma pass results of dose distribution for beams energy of 6, 12 and 20 MeV with cutout sizes of 10×10 , 4×4 , 3×3 , 2×2 and $1 \times 1 \text{ cm}^2$

Cutout size (cm^2)	Percent gamma pass($\gamma_{2\%, 2\text{mm}}$)		
	6 MeV	12 MeV	20 MeV
10x10	97.8	97.5	97.2
4x4	95.6	95.2	94.7
3x3	94.8	93.9	93.2
2x2	93.8	92.6	92.5
1x1	88.6	86.2	86.2

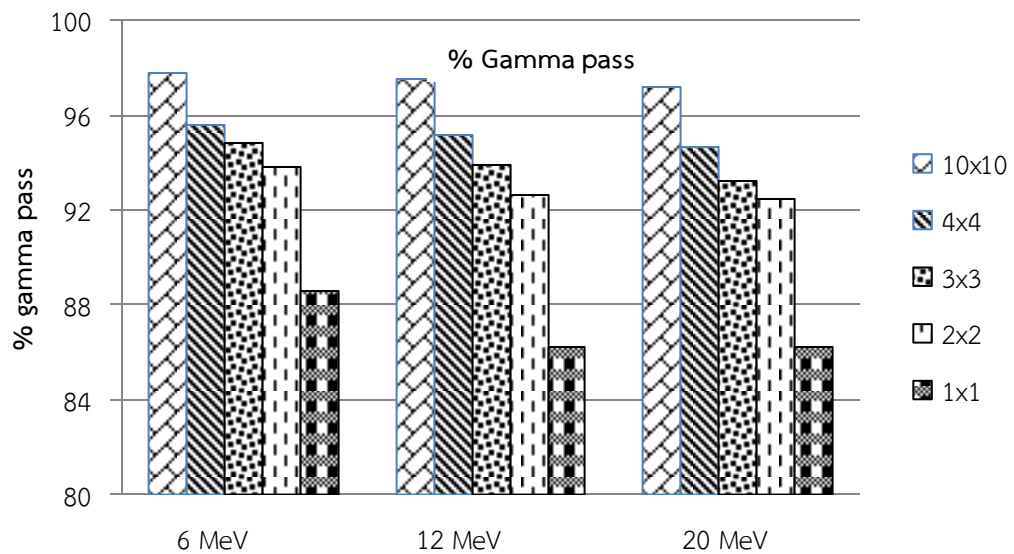


Figure 4. 8. Gamma analysis results of dose distribution for beams energy of 6, 12 and 20 MeV for cutout sizes of 10x10, 4x4, 3x3, 2x2 and 1x1 cm²

The lowest gamma index illustrated at the cutout of 1x1 at 20 MeV, it could be explained from percentage depth dose. The mean difference percentage depth dose of this cutout at 20 MeV was exceeded the 2 mm tolerance, most of different points occurred at the depth beyond R_{50} . That made some gamma index fail on criteria of gamma pass (2%, 2mm) at the below of EDR2 film. However, that effect will be reduced as the field size increasing or energy decreasing, gamma pass will be higher.

4.2. Irregular fields

In clinical practice, the dose in the fields that one side was long and the other side was narrow were changed the same as fields that were narrow in both dimensions. We also investigated such fields, namely 10x1, 10x2, 10x3, 10x4 rectangles, and 1, 2, 3, 4 cm in diameter of circles (C1, C2, C3, C4), and 1, 2, 3, 4 cm in width of L shapes (L1, L2, L3, L4). The measurements and eMC calculations of

output factors for 6, 12 and 20 MeV are shown in Table 4.6. Similar to square shape, the output factors of large field cutout mostly equal to 1.0. For small fields, the output factors were significantly reduced compared with the broad beam distribution.

Table 4. 6. Measurements and eMC calculations of output factors for 6, 12 and 20 MeV for irregular shapes of cutout.

Cutouts	Measurements			eMC Calculations		
	6 MeV	12 MeV	20 MeV	6 MeV	12 MeV	20 MeV
C1	0.61	0.85	0.93	0.71	0.92	0.99
C2	0.83	0.93	0.98	0.87	0.97	1.00
C3	0.93	0.96	0.99	0.95	0.98	0.99
C4	0.98	0.97	0.98	0.99	0.98	0.99
10x1	0.68	0.89	0.99	0.78	0.95	1.04
10x2	0.92	0.93	0.99	0.97	0.97	1.01
10x3	0.97	0.96	0.99	0.99	0.98	0.99
10x4	0.99	0.98	1.01	1.01	0.99	1.01
L1	0.74	0.91	0.97	0.85	0.97	1.02
L2	0.92	0.94	0.98	0.97	0.97	0.99
L3	0.99	0.95	0.99	1.01	0.96	1.00
L4	0.99	0.97	0.98	1.00	0.98	0.99

Table 4.7 is the summary of comparison for output factors, percentage depth dose and dose distribution between measurements and eMC calculations for irregular shapes of cutout. Comparison of output factors were presented by percent difference. The mean distance discrepancies (in mm) between calculated and measured dose evaluated at 5% intervals between 20% and 80% dose range were used for comparison of percentage depth dose, and gamma pass technique for dose distribution. The agreement of eMC calculations with measurements was observed in

case of square fields. The percent difference of output factors were more than 2% in case of cutout C1, C2, C3, 10x1, 10x2, L1, L2, and L3. The mean distance discrepancies for comparison of percentage depth dose presented larger than 2 mm in case of cutout C1, C2, 10x1, and L1. The gamma pass were below 90% in case of cutout C1, 10x1, and L1. For other cutouts, the output factor, percentage depth dose and dose distributions of eMC calculation showed very good agreement to measurements.

Table 4. 7. Comparison for output factors, percentage depth dose and dose distribution between measurements and eMC calculations for irregular shapes of cutout for 6, 12 and 20 MeV

Cut-out	Comparison_OF			Comparison_PDD			Comparison_DD		
	% diff			Δ (mm)			Gamma Pass (%)		
	6MeV	12MeV	20MeV	6MeV	12MeV	20MeV	6MeV	12MeV	20MeV
C1	16.8	8.1	6.2	2.51±1.78	8.02±2.13	12.2±2.25	88.4	88.1	87.6
C2	4.8	4.5	2.5	1.00±0.86	1.24±0.78	2.20±1.96	94.3	92	92.9
C3	2.3	1.7	0.5	0.5±0.67	0.43±1.03	0.71±0.34	94.6	94.2	93.8
C4	1.3	0.8	0.6	0.4±0.56	0.21±0.99	0.61±0.18	95.8	96.1	95.4
10x1	15.2	7.3	4.8	2.24±1.43	6.27±2.28	13.2±3.68	89.7	87.6	87.3
10x2	5.3	4.8	2.2	0.9±0.16	1.16±0.82	1.85±1.24	93.7	93	92.8
10x3	1.9	1.8	0.4	0.4±0.89	0.72±0.81	0.82±1.34	95.2	93.6	94.2
10x4	1.6	1.2	0.4	0.5±0.42	0.47±0.13	0.72±0.98	96.4	96.2	95.5
L1	14.7	6.8	4.7	2.08±1.86	6.15±2.75	13.8±3.03	90.2	87.9	87.7
L2	5.5	3.6	1.4	0.7±0.11	1.45±1.23	1.90±1.86	94.1	92.6	92.4
L3	2.3	1.2	0.7	0.2±0.91	0.83±1.27	1.00±1.03	95.4	94.8	93.4
L4	0.8	0.7	0.8	0.2±0.08	0.62±0.81	0.90±0.07	96.8	96.3	95.8

The square and irregular shapes of 2 and 3 cm at one side of cutout were presented in the same figure and shown in Figure 4.9(a-b) for output factors, figure 4.10(a-b) for percentage depth dose and Figure 4.11(a-b) for dose distribution, respectively. Similar to output factors and percentage depth dose of standard fields, the output factor difference of irregular shapes were also lesser difference when the energy was increasing. In contrast, the percentage depth dose difference of irregular shape showed the larger mean distance discrepancies (in mm) with the higher energy as shown in Figure 4.10. Percentage gamma pass were also increasing as the fields were increasing.

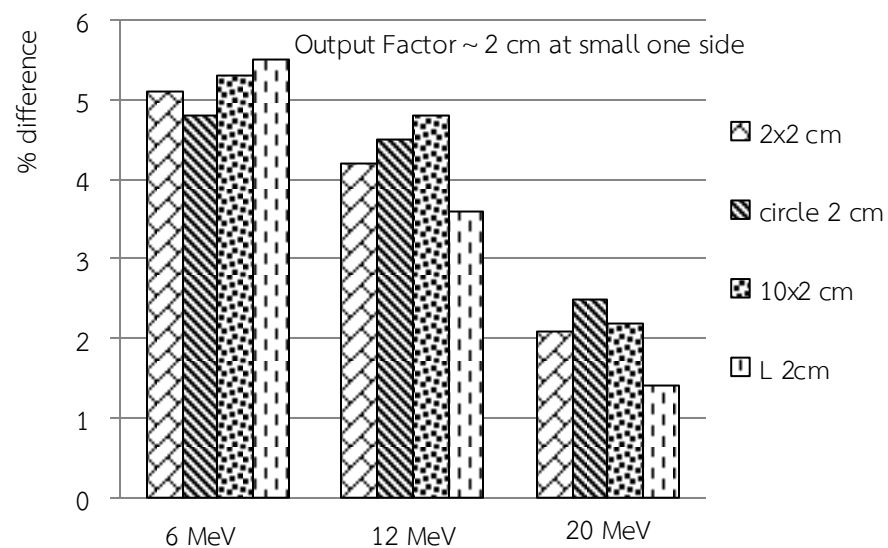


Figure 4.9- a. Comparison of output factor between calculated and measured for standard and irregular shape of 2 cm at small one side.

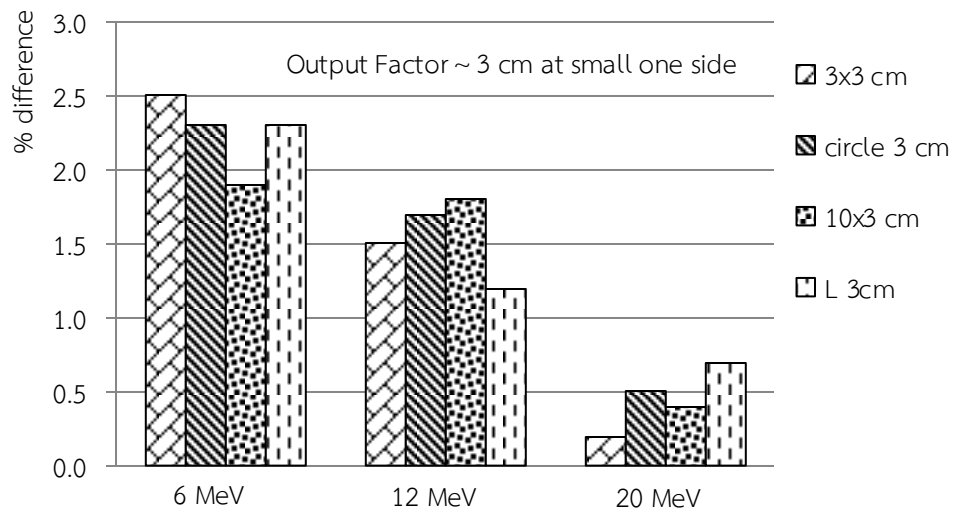


Figure 4.9- b. Comparison of output factor between calculated and measured results for standard and irregular shape of 3 cm at small one side.

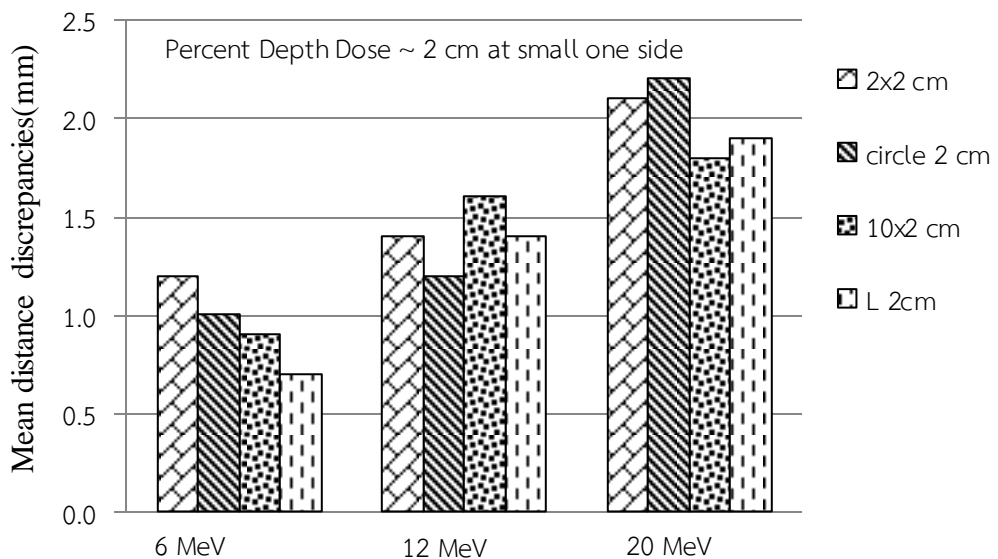


Figure 4.10- a. Mean distance discrepancies in PDD (in mm) between calculated and measured dose evaluated at 5% intervals between 20% and 80% dose range for standard and irregular shape of 2 cm at small one side.

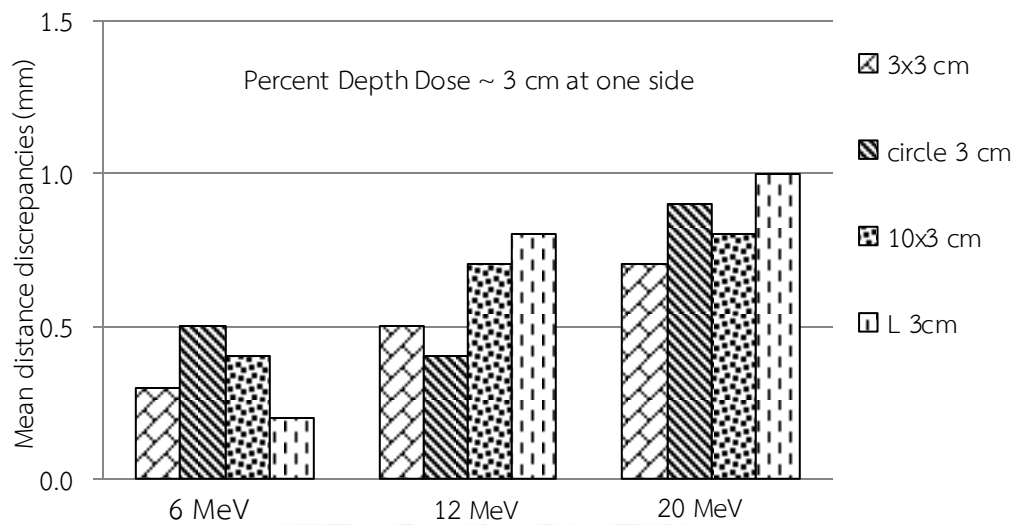


Figure 4.10- b. Mean distance discrepancies in PDD (in mm) between calculated and measured dose evaluated at 5% intervals between 20% and 80% dose range for standard and irregular shape of 3 cm at small one side

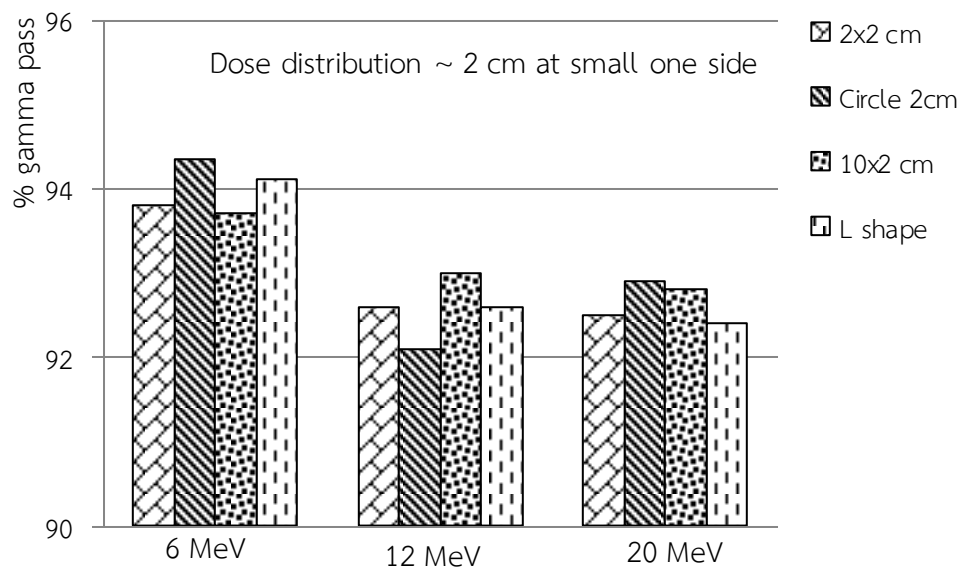


Figure 4.11- a. Comparison Dose Distribution between calculated and measured results for standard and irregular shape of 2 cm at small one side.

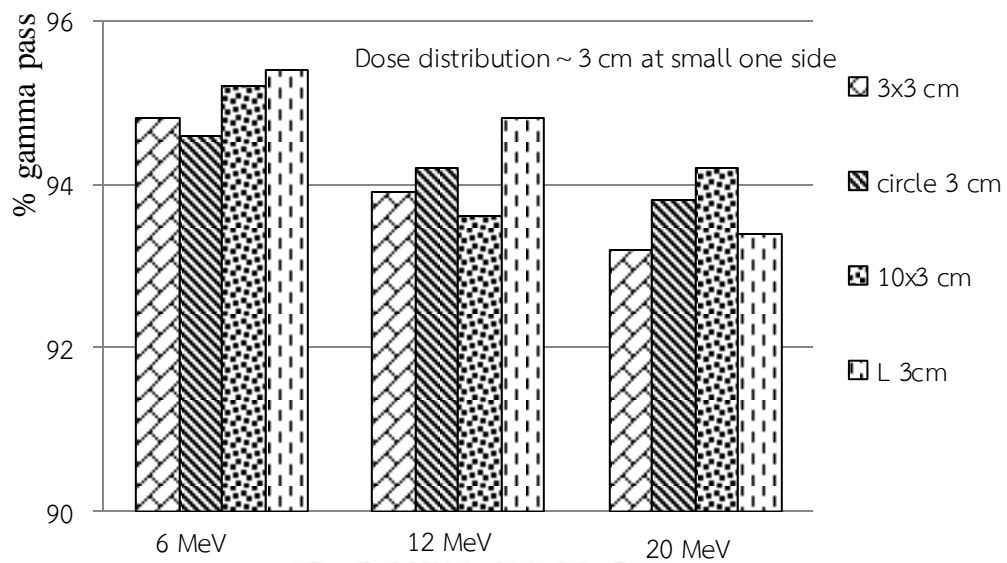


Figure 4.11- b. Comparison Dose Distribution between calculated and measured results for standard and irregular shape of 3 cm at small one side.

To compare output factors, percentage depth dose, dose distribution of irregular with standard shapes of cutout, Table 4.8 is the summary in case of square fields such as 1x1, 2x2, 3x3 and 4x4. Table 4.9 was performed from Table 4.7 and Table 4.8 to compare between irregular and standard shapes.

Table 4. 8. Comparison for output factors, percentage depth dose, dose distribution between measurements and eMC calculations for 1x1, 2x2, 3x3 and 4x4 cm².

Cut-out	Comparison_OF			Comparison_PDD			Comparison_DD		
	% diff			Δ (mm)			Gamma Pass (%)		
	6MeV	12MeV	20MeV	6MeV	12MeV	20MeV	6MeV	12MeV	20MeV
1x1	16.4	7.6	5.8	2.26±0.86	7.35±1.27	12.8±2.23	88.6	86.2	86.2
2x2	5.1	4.2	2.2	1.25±0.12	1.44±0.04	2.11±0.47	93.8	92.6	92.5
3x3	2.5	1.5	0.2	0.30±0.15	0.48±0.09	0.67±0.15	94.8	93.9	92.5
4x4	1.6	0.4	-0.9	0.39±0.08	0.27±0.05	0.64±0.11	97.8	97.5	97.2

Table 4. 9. Comparison between square and irregular shapes in term of agreement between measurements and eMC calculations for output factors, percentage depth dose and dose distribution

Cut-out	Comparison_OF			Comparison_PDD			Comparison_DD		
	% diff Irrigular - Square			Δ (mm) Irrigular - Square			Gamma Pass (%) Irrigular - Square		
	6MeV	12MeV	20MeV	6MeV	12MeV	20MeV	6MeV	12MeV	20MeV
C1	0.4	0.5	0.4	0.25	0.67	-0.6	-0.2	1.9	1.4
C2	-0.3	0.3	0.3	-0.25	-0.24	0.09	0.5	-0.6	0.4
C3	-0.2	0.2	0.3	0.2	-0.08	0.03	-0.2	0.3	1.3
C4	-0.3	0.4	1.5	0.01	-0.07	-0.04	-2	-1.4	-1.8
10x1	-1.2	-0.3	-1	-0.02	-1.08	0.4	1.1	1.4	1.1
10x2	0.2	0.6	0	-0.35	0.16	-0.31	-0.1	0.4	0.3
10x3	-0.6	0.3	0.2	0.1	0.22	0.13	0.4	-0.3	1.7
10x4	0	0.8	1.3	0.11	0.13	0.06	-1.4	-1.3	-1.7
L1	-1.7	-0.8	-1.1	-0.18	-1.2	1	1.6	1.7	1.5
L2	0.4	-0.6	-0.8	-0.55	-0.04	-0.21	0.3	0	-0.1
L3	-0.2	-0.3	0.5	-0.1	0.32	0.33	0.6	0.9	0.9
L4	-0.8	0.3	1.7	-0.19	0.33	0.26	-1	-1.2	-1.4

All of values in Table 4.9 were less than 2% for output factor and gamma pass, and less than 2 mm for percentage depth dose. These results suggested that there were no significant differences between standard and irregular shape in terms of comparison between calculated and measured results. As long as the shorter

dimension of a shaped field is smaller than 3.0 cm, calculated dose distribution and MUs can be differed significantly from the measurement.



CHAPTER 5

CONCLUSIONS

The comparison between eMC calculations and measurements in terms of beam profiles, percentage depth doses, and output factors for small cutout sizes with several shapes show the good agreement as followings:

1. The agreement between calculated and measured percentage depth dose (within 1%), beam profile (within 1 mm), and dose distribution (greater than 97%) for a $10 \times 10 \text{ cm}^2$ open field are excellent, there by validating of Monte Carlo calculation.

2. The calculation of percentage depth dose match the measurement results within 2 mm for all energies of the square field sizes, except the $2 \times 2 \text{ cm}^2$ cutout, the mean distance discrepancies of 2.1 mm for 20 MeV, and the $1 \times 1 \text{ cm}^2$ cutout that also shows the largest deviation of 12.8 mm at 20 MeV.

3. All comparisons of beam profiles match well within 2% dose difference and 2 mm distance to agreement in the case of square field cutout from 1×1 to $10 \times 10 \text{ cm}^2$.

4. The agreement of output factors are within 2% for cutout sizes from 3×3 to $10 \times 10 \text{ cm}^2$ for all energies, except 6 MeV for $3 \times 3 \text{ cm}^2$ cutout that shows 2.5% deviation. For $2 \times 2 \text{ cm}^2$ cutout, the calculated output factors deviate from the measurement within 5.1%. The $1 \times 1 \text{ cm}^2$ cutout presents the worst results with percent differences above 5%.

5. The dose distribution agreement between measured and calculated values is excellent for the 10x10, 4x4, 3x3 and 2x2 cm² cutouts, with greater than 92.5% passing of the gamma criteria of 2% / 2mm for all energies tested. The 1x1 cm² cutout shows poor results, the numbers of pixels passing our gamma requirements are below 90% for all the energies tested.

6. The accuracy of eMC in term of percentage depth dose has relationship to percent gamma pass of dose distribution deeply. In small field of electron beam, the percentage depth dose is more accuracy for low energy (6 MeV). This makes percent gamma pass is increasing when energy reducing.

7. For comparisons between measurements and eMC calculations of irregular shapes of cutout, the percent difference of output factors are more than 2% in case of cutout C1, C2, C3, 10x1, 10x2, L1, L2, and L3, the mean distance discrepancies for comparison of percentage depth dose present larger than 2 mm in case of cutout C1, C2, 10x1, and L1, the gamma pass are below 90% in case of cutout C1, 10x1, and L1. For other cutouts, the output factor, percentage depth dose and dose distributions of eMC calculation show very good agreement to measurements.

8. The irregular shape of only one small side of the fields have more influence effect in the percentage depth dose, output factors and dose distributions

9. The minimum cutout size that eMC can accurately predict beam profile, percentage depth doses, and output factors is as small as a 3 cm diameter for energies in the 6 to 20 MeV range at 100 cm SSD, it is consistent with the recommendation by Popple et al. When a cutout size or any dimension of a shaped

field is smaller than 3.0 cm, calculated dose distribution and output factor are significantly different from the measurement.

10. In clinical treatment, the field of cutouts which are long and narrow less than 2 cm in width of cutout are used to treat the keloid. However, in this case electronic equilibrium is not obtained and Monte Carlo algorithm do not permit the calculation of electron scattering correctly. Because of this reason, the comparison of this result between eMC and calculation are not accurate. The small cutouts can be used for treatment but one should notice that treatment planning system will not predict the dose accuracy.

11. When Monte Carlo based treatment planning systems is implemented into the clinical practice, one should pay particular attention to those fields with cutout sizes smaller than 3 cm in diameter with low energies. In such cases, a special dosimetry (e.g. output factor, depth-dose, and isodose distribution) should be measured individually and used for the treat patients.

REFERENCES

1. Khan, F.M., Electron beam therapy. The physics of radiation therapy. Baltimore: Williams and Wilkins, 2(1994):353-374.
2. Klevenhagen, S.C., Electron interactions with matter. Physics of electron beam therapy. Med Phys Handbook 13 (1985):37-88.
3. Nordic Association of Clinical Physics (NACP). Procedures in external radiation therapy dosimetry with electron and photon beams with maximum energies between 1 and 50 MeV. Acta Radio1 (1980):19-55.
4. Markus, B. Beitrage zur Entwicklung der Dosimetrie schneller Elektronen Strahlentherapie (1964); 123-350.
5. Nusse, M. Factors affecting the energy-range relation of fast electrons in aluminum. Pphys Med Biol (1969):14-315.
6. Harder, D. Schulz, H.J., Some new physical data for electron beam dosimetry. Proceedings of the European Congress of Radiology. Amsterdam: Excerpta Medica, 1971.
7. Harder, D., Montreux, Zup-pinger, A., Poretti, G., eds. Symposium on high-energy electrons. Berlin: Springer-Verlag, (1965):260.
8. Zhang, G.G., Roger, D.W.O. Montecarlo investigation of electron beam output factor versus size of square cutout. Med Phys 26(1999):743-749.

9. Almond, P.R. Radiation physics of electron beams. Clinical applications of the electron beam. New York: John Wiley & Sons, (1976):50
10. Klevenhagen, S.C. Exploring electron beam characteristics. Physics and dosimetry of therapy electron beam. Wisconsin Med Phys 1(1993):410-422
11. Radiation therapy accessories. Custom blocking, Med-Tec Inc., 1995-1996.
12. Biggs, P.J., Boyer, A.L., Doppke, K.P. Electron dosimetry of irregular fields on the Clinac-18. Int J Radiat Oncol Biol Phys 1 (1979):435:433.
13. Mills, M.D., Hogstrom, K.R., Almond PR. Prediction of electron beam output factors. Med Phys 1(1982): 9:60.
14. ICRU. Radiation dosimetry: electron beams with energies between 1 and 50 MeV. Report No. 35. Bethesda, MD: International Commission on Radiation Units and Measurements, 1984.
15. Low, D.A., Harms, W.B., Sasa, M., Purdy, J.A. A technique for the quantitative evaluation of dose distributions. Med Phys 25(1998):656–661.
16. Jursinic, P.A., and Nelms, B.E., A 2-D diode array and analysis software for verification of intensity modulated radiation therapy delivery, Med. Phys 30 (2003):870-879
17. Shi, J., Simon, W.E., Zhu, T.C., Modeling the instantaneous dose rate dependence of radiation diode detectors, Med. Phys 30 (2003): 2509-2519
18. Saini, A.J.S., and Zhu, T.C., Dose rate and SSD dependence of commercially available diode detectors, Med. Phys 31 (2004): 914-9

19. Khan, F.M., Doppie, K.P., Hostrom, K.R., et.at. Clinical electron beam dosimetry :
Report of AAPM Radiation Therapy Task Group No 25. Med Phys 18
(1991):73-108.
20. Feldman, A., Almeida, C.E., Almond, P.R. Measurement of electron beam energy
with rapid processed film. Med phys 1 (1974):74-76.
21. Rustgi, S.N., Working, W.R. Dosimetry of small field electron beams. Med Dosim
1 (1992; 1792):107-110.
22. Shrama, S.C., Wilson, D.L., Jose, B. Dosimetry of small fields of 20 electron beam.
Med Phys 11(1984):697-702.
23. Sternick, E., Orton, C.G., Bagne, F. Proceedings of the Practical Aspects of
Electron Beam Treatment Planning Symposium. Cincinnati, Ohio. Junly
1977.
24. Hogstrom, K.R., Starkschal, G., Shiu, A.S. Dose calculation algorithms for electron
beams. Advances in RadiolOncol.Phys: Dosimetry, Treatment Planning
and Brachytherapy. American Institute of Physics Monograph,1992.
25. Lax, I., Brahme, A. Collimation of high energy electron beams. ActaRadiolOncol.
19(1980):199-207.
26. Verhaegen, F. Monte carlo calculation of output factors for circular, rectangular,
and square fields of electron accelerators (6-20 MeV). United Kingdom,
26 march 2001.

27. Zhigang, X. Evaluation of the eclipse electron Monte Carlo dose calculation for small field. Stony Brook University Medical Center, New York .
RadiolOncol 11 (May 2009):56-68
28. Evans and Schreiner, L. J. A simple technique for film dosimetry. Radiother. Oncol 23 (1992): 265–267.
29. Hale, J. I., Kerr, A. T., and Shragge, P. C. Calibration of film for accurate megavoltage photon dosimetry, Med. Dosimetry 19 (1994): 43–46.
30. Inhwon, J. Yeo., Chris Wang, C.K., and Sandra, E. Burch. A filtration method for improving film dosimetry in photon radiation therapy. Med Phys 24 (Dec 1997): 1943–1953.
31. Robar, J. L and Clark, B. G. The use of radiographic film for linear accelerator stereotactic radiosurgical dosimetry. Med Phys 26 (1999):2144–2150.
32. Popple, R.A., Weinber, R., Antolak, J.A., et al. Comprehensive evaluation of a commercial macro Monte Carlo electron dose calculation implementation using a standard verification data set. Med Phys 33 (2006):1540–1551.
33. Heidelberg, Germany. IAEA. Technical Reports Series No. 430. Commissioning and Quality Assurance. Computerized Planning Systems for Radiation Treatment of Cancer 1 (2000):19-21
34. Brian, J., Mcparland. Parameterization of the electron beam output factors of a 25-MeV linear accelerator. Department of Med Phys, Dalhousie University, Canada.

VITA

NAME Mr. Minh Bui Hoang

DATE OF BIRTH 22 May 1988

PLACE OF BIRTH Ho Chi Minh city, Vietnam

INSTITUTION ATTENDED University of Science, 2010:
Bachelor of Science
(NuclearPhysics)

Chulalongkorn University, 2014:
Master of Science
(Medical Imaging)

HOME ADDRESS C2/10, Quarter 3, Tan Tuc Town,
BinhChanh District, Ho Chi Minh City,
Vietnam

Tel. (+84) 936 124914



จุฬาลงกรณ์มหาวิทยาลัย
CHULALONGKORN UNIVERSITY